Quantum chaos applications: from simple models to quantum computers and Google matrix

Dima Shepelyansky (CNRS, Toulouse)
www.quantware.ups-tlse.fr/dima

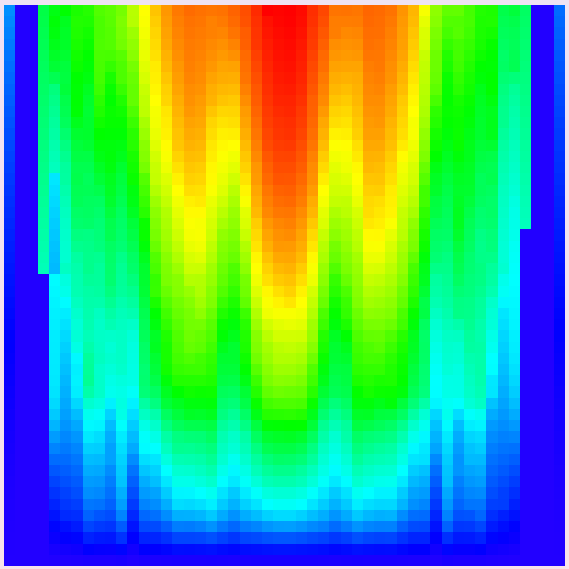
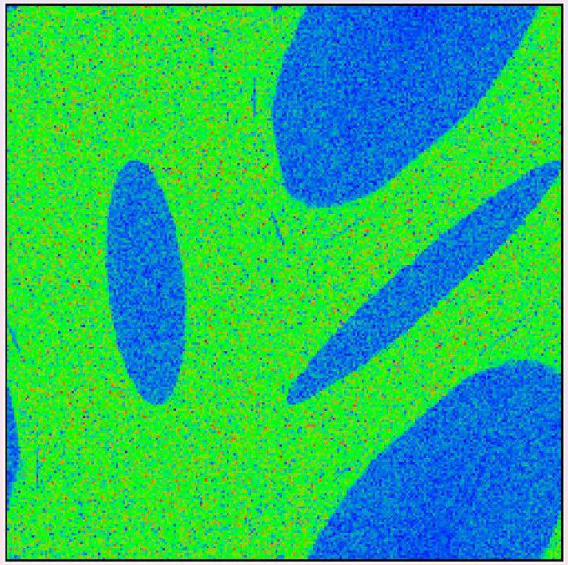
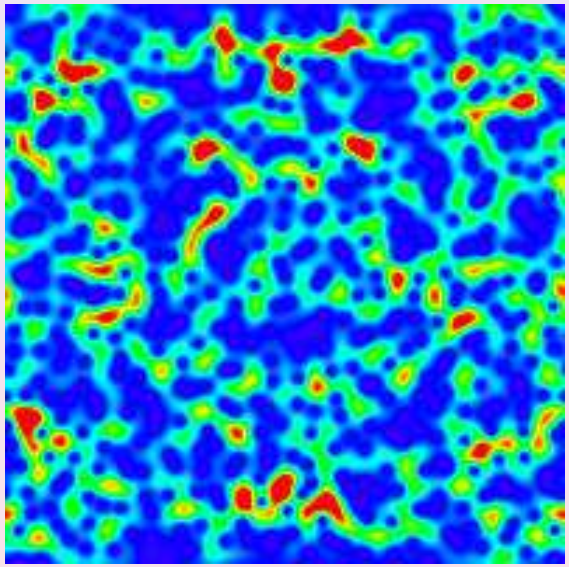

L1: Simple models of classical and quantum chaos
L2: Anderson localization in presence of nonlinearity and interactions
L3: Quantum chaos in many-body systems and quantum computers
L4: Google matrix and directed networks

Quantum chaos in many-body systems

Wigner 1955-57 => Random Matrix Theory
to describe "the properties of the wave functions of quantum mechanical systems which are assumed to be so complicated that statistical considerations can be applied to them"
Wigner surmise $P_W(s) = (\pi s/2)\exp(-\pi s^2/4)$
vs. Poisson distribution $P_P(s) = \exp(-s)$

Onset of quantum chaos in systems with two-body interactions:
spacing between adjacent energy levels drops exponentially with number of particles n: $\Delta_n \propto \exp(-n)$.
Interaction induced coupling, two-body matrix element U_s.

Spacing between directly coupled states: $\Delta_c \gg \Delta_n$.

Åberg criterion for onset of quantum chaos:
$U_s \approx \Delta_c \gg \Delta_n$

Åberg (1990), (1992); DS, Sushkov (1997); Jacquod, DS (1997)

Three interacting particles in a box

N one-particle levels with average spacing $\Delta \sim V/N$
(e.g. 2d Anderson model of size $L \ll \ell$)

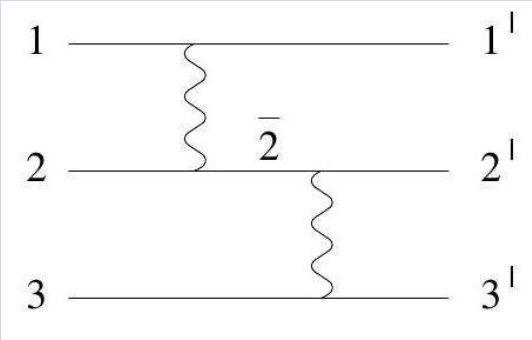

Interaction coupling matrix element $U_2 \sim U_s$
Density of two-particle states
$\rho_2 \approx 1/\Delta_2 \sim N^2/V \sim N/\Delta$
Density of two-particle states
$\rho_3 \approx 1/\Delta_3 \sim N^3/V \sim \Delta/{\Delta_2}^2$

The matrix element between initial three-body state $|123>$ and final state $|1'2'3'>$ is given by diagram presented in Fig. with intermediate state $|1'\bar{2}3>$

$$U_{s3} = \sum_{\bar{2}} \frac{<12|U_{12}|1'\bar{2}><\bar{2}3|U_{23}|2'3'>}{(E_1+E_2+E_3-E_{1'}-E_{\bar{2}}-E_3)} \sim \frac{{U_s}^2}{\Delta} ;$$

the summation is carried out only over single particle states $\bar{2}$ and hence the minimal detuning in the dominator is about Δ. Mixing of 3-particle levels takes place when $U_{s3} \sim {U_s}^2/\Delta \sim \Delta_3 \sim {\Delta_2}^2/\Delta$. Hence the transition from Poisson to Wigner-Dyson statistics for three interacting particles takes place at

$$U_s \sim \Delta_2 \gg \Delta_3$$

DS, Sushkov (1997)

Two-body random interaction model (TBRIM)

random two-body matrix elements $\pm U$ in a system of m one-particle orbitals of spacing Δ, with n fermions (French, Wong, Phys. Lett. B **33**, 447 (1970); **35**, 5 (1971); Bohigas, Flores Phys. Lett. B **34**, 261 (1971); **35**, 383 (1971) Flambaum, Gribakin, Izrailev, PRE **53**, 5729 (1996))

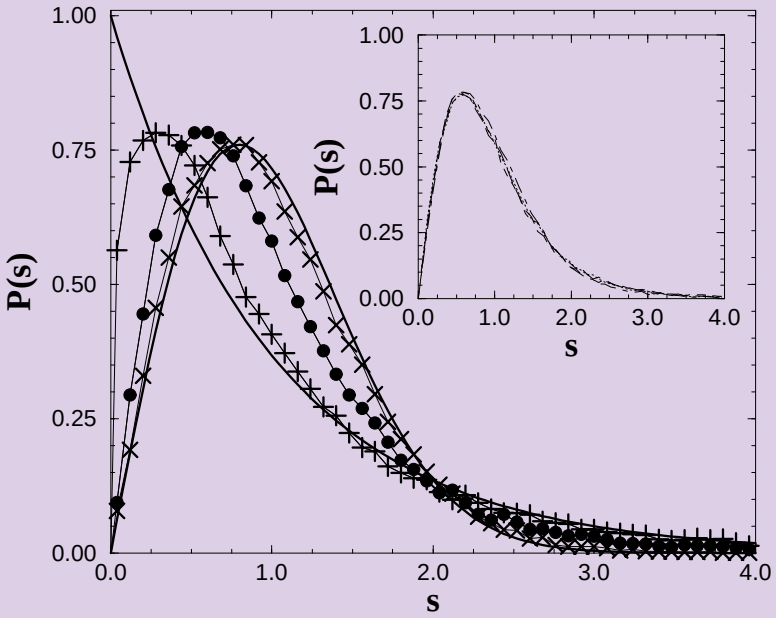

Transition from Poisson to Wigner-Dyson statistics in the TBRIM for $m = 12$, $n = 6$: $U/\Delta = 0.01$ and $\eta = 0.93$ (+); $U/\Delta = 0.055$ and $\eta = 0.3$ (•); $U/\Delta = 0.13$ and $\eta = 0.063$ (x). Full lines show the Poisson and the Wigner-Dyson distributions. Insert shows $P(s)$ at fixed $\eta = 0.3$ for half-filling $\nu = n/m = 0.5$ and $n = 4, 5, 6, 7$.

The total number of multiparticle states is $N = m!/(n!(m-n)!)$, a multiparticle state is coupled with $K = 1 + n(m-n) + n(n-1)(m-n)(m-n-1)/4$ states in band $B = (2m-4)\Delta$; [$\eta = \int_0^{s_0}(P(s) - P_W(s))ds / \int_0^{s_0}(P_P(s) - P_{WD}(s))ds$, intersection point $s_0 = 0.4729...$; $\eta = 1$ for $P(s) = P_P(s)$, 0 for $P(s) = P_W(s)$] Jacquod, DS (1997)

Quantum chaos in TBRIM

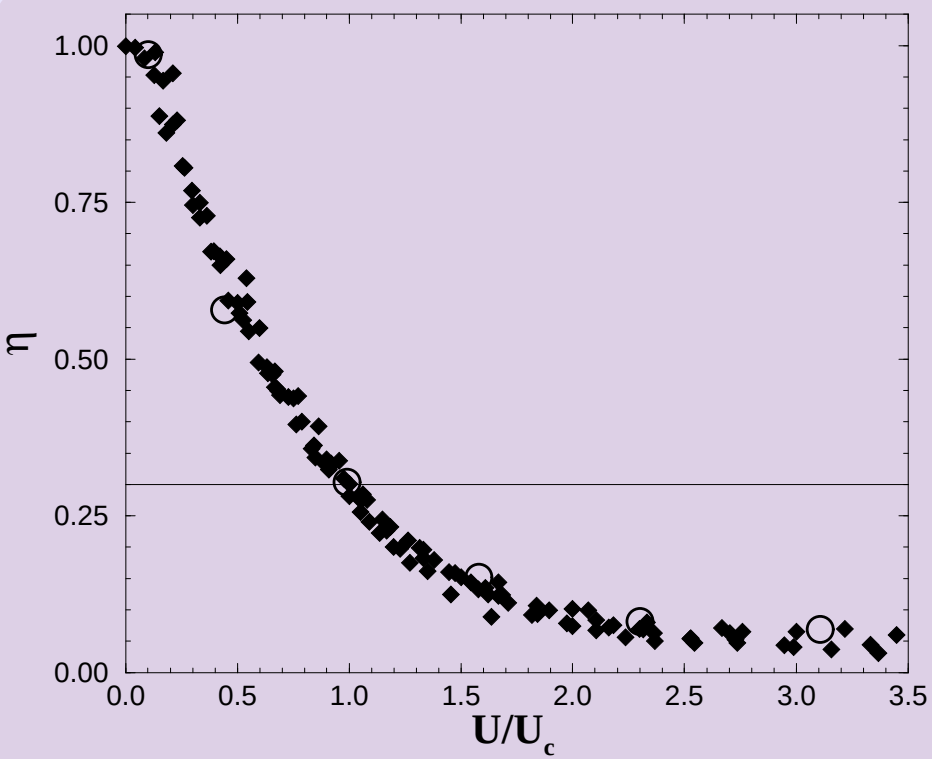

$2 \leq n \leq 8,\ 4 \leq m \leq 80$

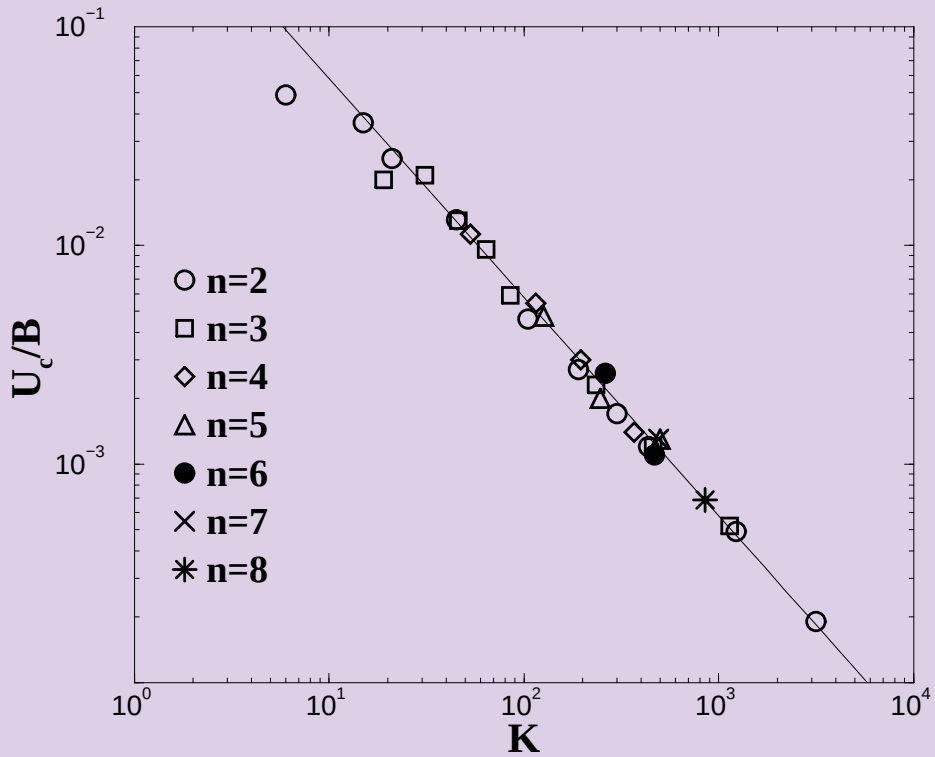

$1/40 \leq n/m \leq 1/2,\ C = 0.58$

$U > U_c = CB/K \approx 2C/\rho_2 n^2$ => Quantum Chaos border

Jacquod, DS (1997)

Dynamical thermalization in finite Fermi systems

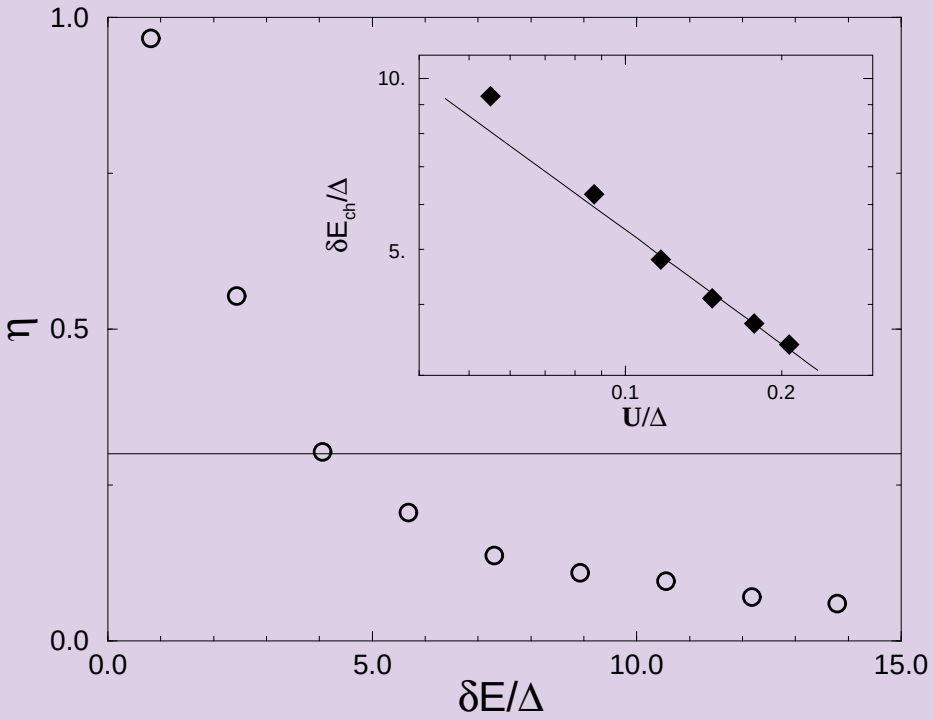

exitation energy above ground state $\delta E \approx T\,\delta n$ with temperature T; density of effectively coupled TIP states $\rho_{2ef} \sim \epsilon/\Delta^2$, number of excited electrons $\delta n \sim Tn/\epsilon_F \sim T/\Delta$ with $\rho_{2ef} \sim T/\Delta^2$
$n = 6$, $U/\Delta = 0.15$;
inset: $\eta = 0.3$, line is theory at $C = 1.08$

$U > U_c \approx C/\rho_2 n^2 \approx C/(\rho_{2ef}\delta n)^2$ => $T_c = C\Delta(\Delta/U)^{1/3}$

$\delta E > \delta E_{ch} \approx T\,\delta n \approx C\Delta(\delta/U)^{2/3} \approx g^{2/3}\Delta$ => thermalization border
(in metals $U \approx \Delta/g$, $g \gg 1$ conductance)

Åberg (1990); Jacquod, DS (1997)

Breit-Wigner width and participation ratio

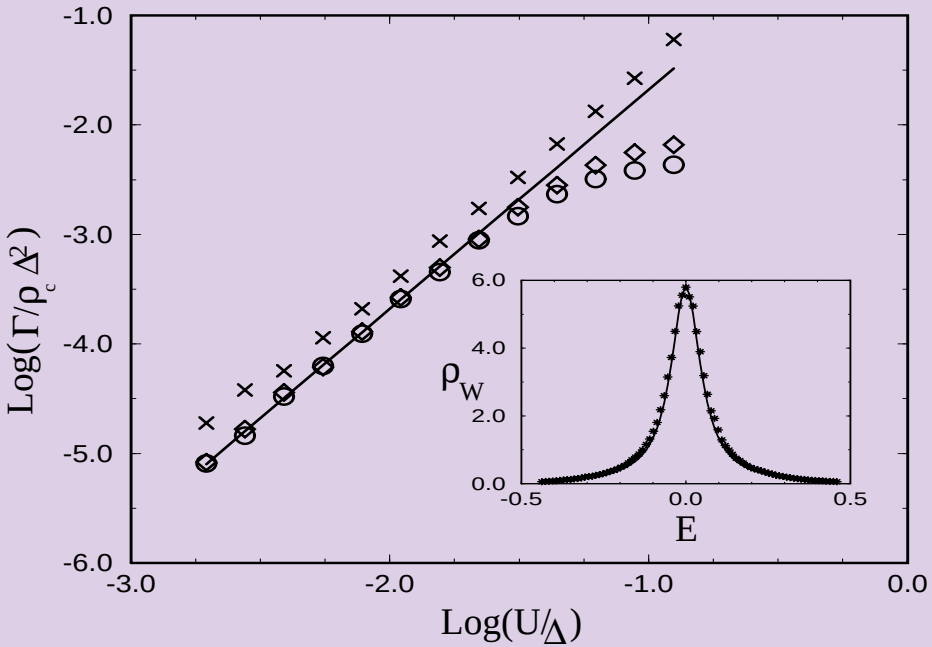

$n/m = 3/17; 3/130; 4/60$

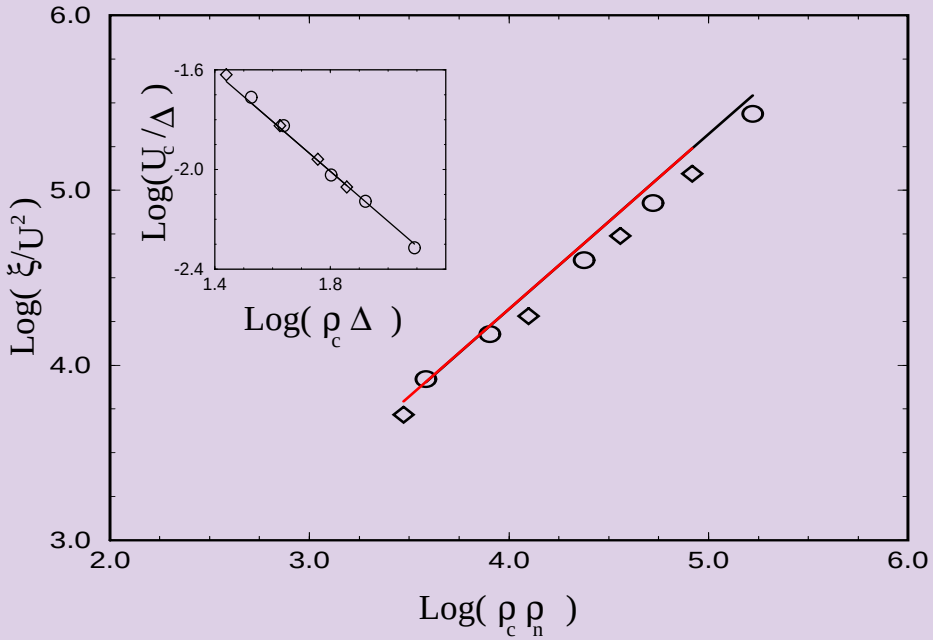

$n = 3, 4; 30 \leq m \leq 130$

Breit-Wigner distribution

$\rho_W(E - E_n) = \sum_\lambda |\psi_\lambda(n)|^2 \delta(E - E_\lambda) = \Gamma/[2\pi((E - E_n)^2 + \Gamma^2/4)]$

Fermi golden rule: $\Gamma = 2\pi < U^2 > \rho_c = 2\pi U^2 \rho_c/3$

number of populated states IPR: $\xi \approx \Gamma \rho_n \approx 2U^2 \rho_c \rho_n$

Georgeot, DS (1997)

Quantum compacton vacuum

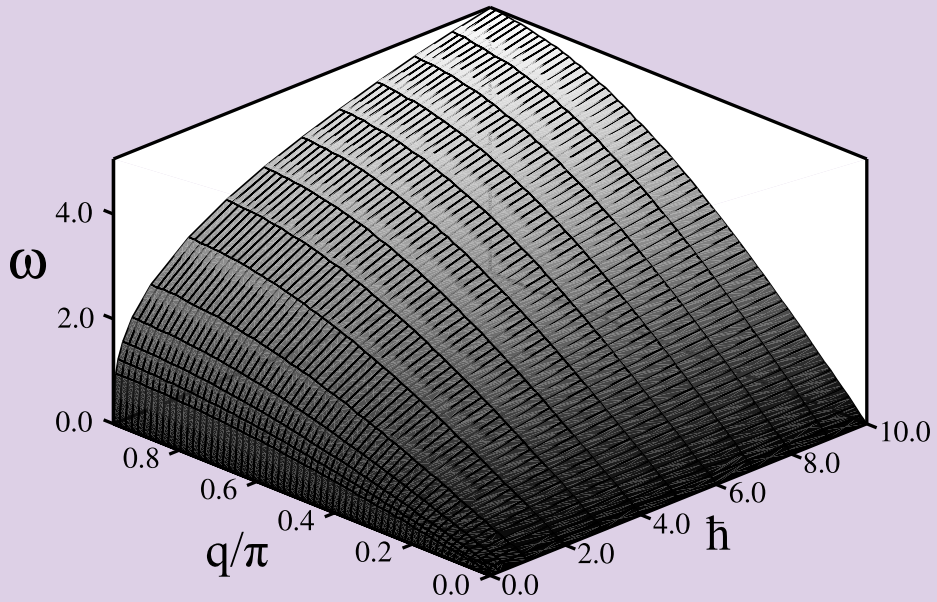

Quantum compacton chain:
$\hat{H} = \sum_{l=1}^{N} [\hat{p}_l^2/2 + (\hat{x}_l - \hat{x}_{l-1})^4/4]$ Classical system: Newton cradle => chaotic at arbitrary small energy (Ahnert, Pikovsky (2009))

Quantum system: phonon type exitations above ground state; sound velocity
$\omega = cq; \quad c \sim \alpha^{2/3}\hbar^{2/3}$ (Zhirov, Pikovsky, DS (2011))

Quantum chaos & quantum computers

- Quantum computer hardware: static properties, imperfections effects
- Main quantum alorithms: fast Fourier transform, Shor algorithm, Grover algorithm
- Quantum algorithms of simple classical/quantum maps: tent map, Arnold cat map, sawtooth map, Chirikov standard map (polynomial number of gates)
- Effects of imperfections and errors, fidelity decay: tent map, sawtooth map, Grover, Shor algorithms
- Experiment of Cory group at MIT: dynamical localization in the quantum sawtooth map
- Arnold cat map on QC with 20 qubits (128×128), time inversion after 10 and 200 iterations =>

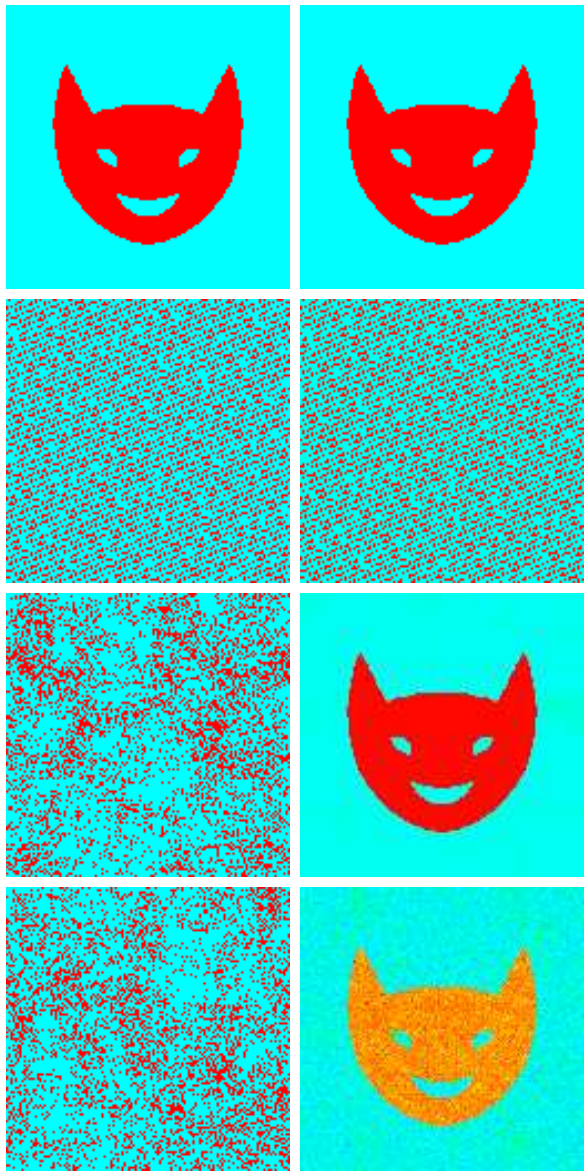

Steane (1998); Nielson, Chuang (2000)

Quantum hardware melting induced by quantum chaos

The quantum computer hardware is modeled as a (one)two-dimensional lattice of qubits (spin halves) with static fluctuations/imperfections in the individual qubit energies and residual short-range inter-qubit couplings. The model is described by the many-body Hamiltonian

$$H_S = \sum_i (\Delta_0 + \delta_i)\sigma_i^z + \sum_{i<j} J_{ij}\sigma_i^x \sigma_j^x ,$$

where the σ_i are the Pauli matrices for the qubit i, and Δ_0 is the average level spacing for one qubit. The second sum runs over nearest-neighbor qubit pairs, and δ_i, J_{ij} are randomly and uniformly distributed in the intervals $[-\delta/2, \delta/2]$ and $[-J, J]$, respectively.

Quantum chaos border for quantum hardware:

$$J > J_c \approx \Delta_c \approx 3\delta/n_q \gg \Delta_n \sim \delta 2^{-n_q}$$

Emergency rate of quantum chaos:

$$\Gamma \sim J^2/\Delta_c .$$

(B.Georgeot, DS (2000))

Quantum hardware melting induced by quantum chaos

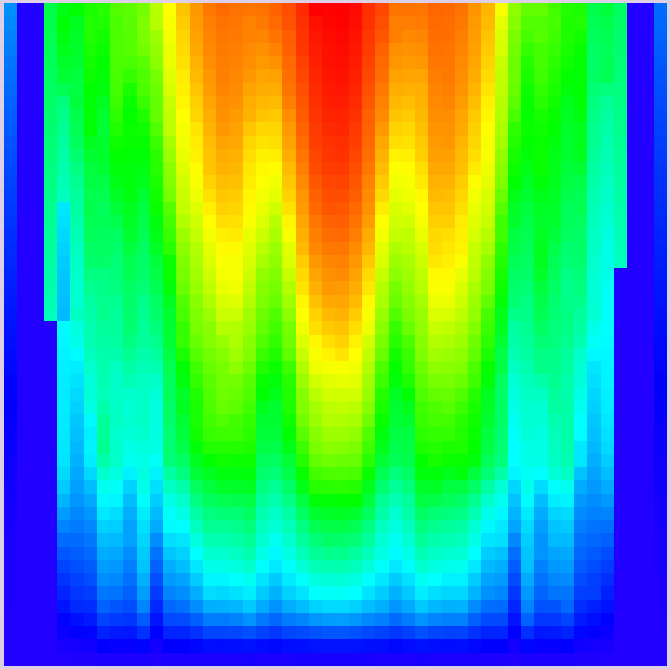

Quantum computer melting induced by inter-qubit couplings. Color represents the level of quantum eigenstate entropy S_q (red for maximum $S_q \approx 11$, blue for minimum $S_q = 0$). Horizontal axis is the energy of the computer eigenstates counted from the ground state to the maximal energy ($\approx 2n_q\Delta_0$). Vertical axis gives the value of J/Δ_0 (from 0 to 0.5). Here $n_q = 12$, $J_c/\Delta_0 = 0.273$, and one random realization of couplings is chosen.

What are effects of quantum many-body chaos on the accuracy of quantum computations?
Static imperfections vs. random errors in quantum gates of a quantum algorithm.

(B.Georgeot, DS (2000))

Quantum hardware melting in time

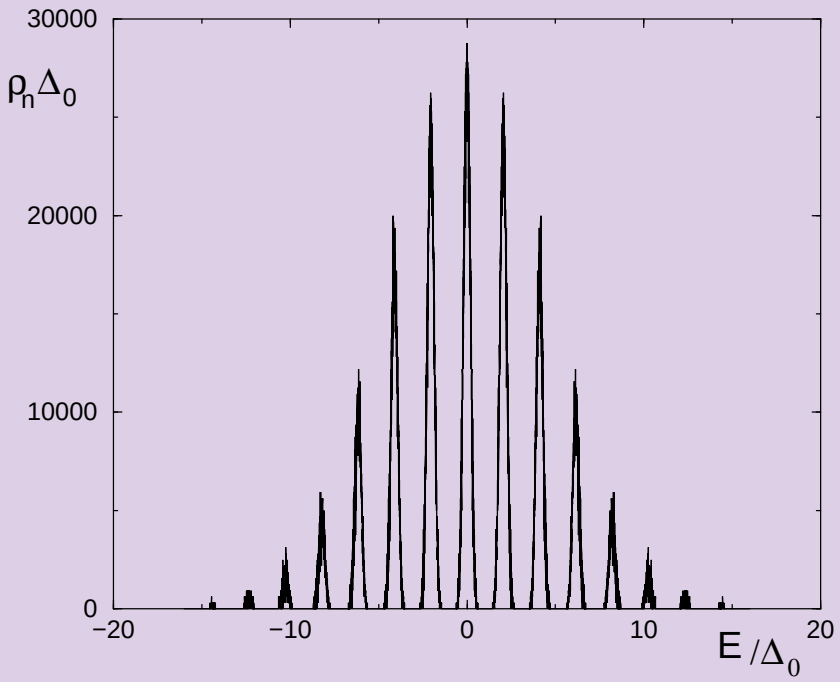

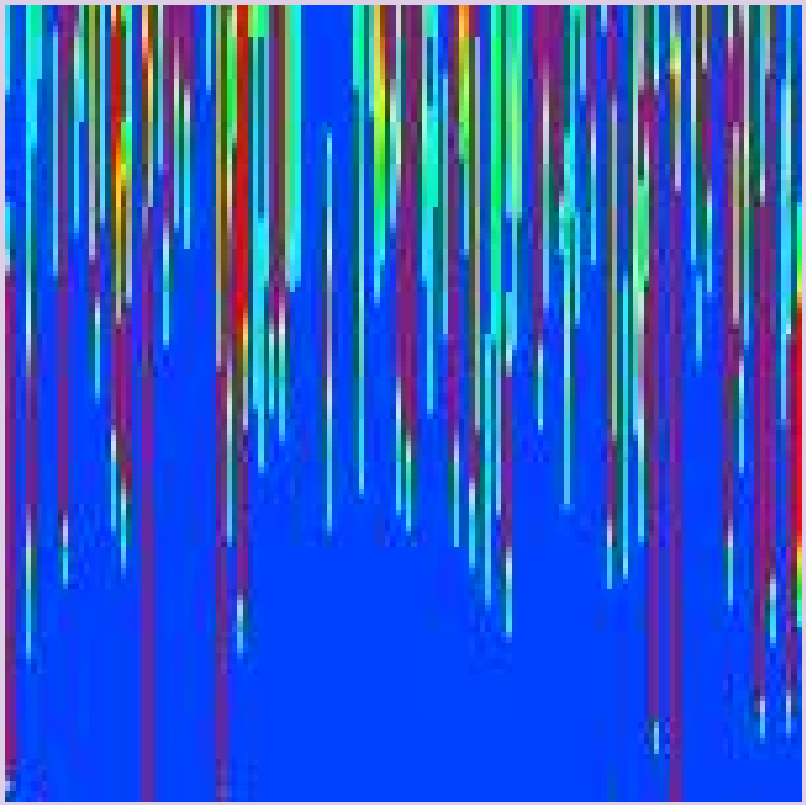

Left: density of states $J = 0, \delta = 0.2\delta, n = 16$

Right: time explosion of quantum chaos in the quantum register: color represents the value of the projection probability of an initial state on the quantum register states ordered in energy (150 states in x-axis); time is in y-axis from $0 \leq t\delta \leq 2$; the initial state is the superposition of two quantum register states; $n = 16$, $J/\delta = 0.4$ ($J/\delta > J_c/\delta = 0.22$): $t > 1/\Gamma$

Dynamical thermalization of QC

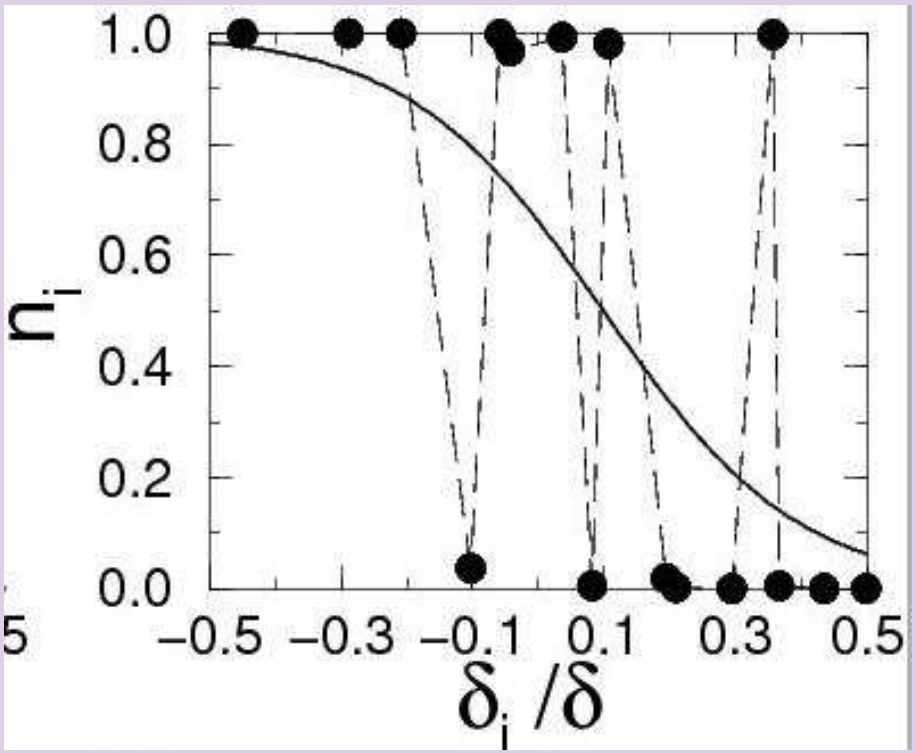

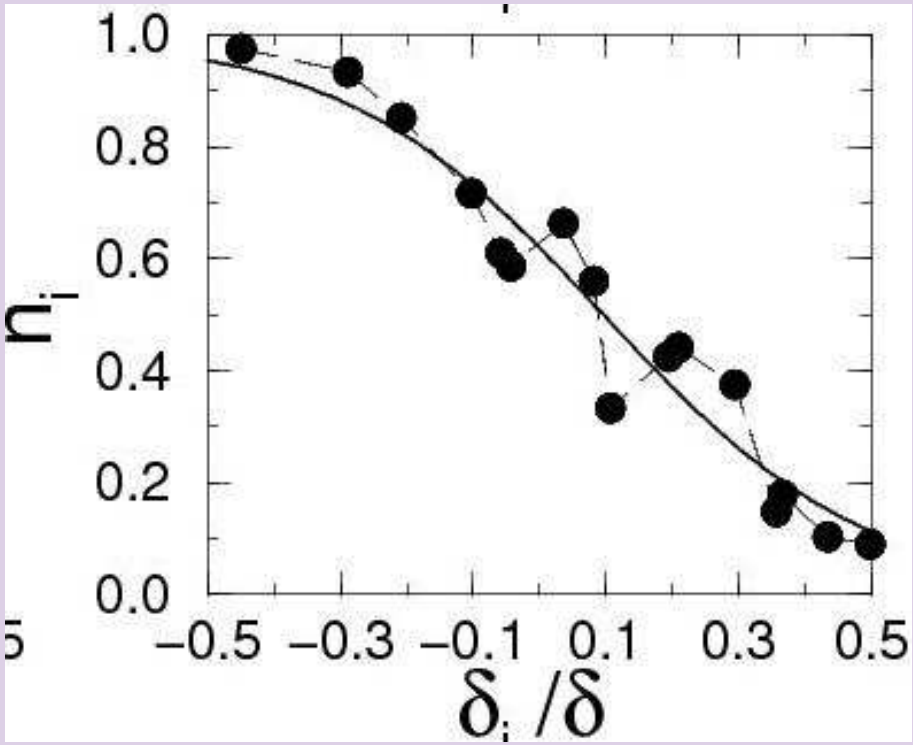

Example: Quantum computer with $n_q = 16$ qubits, central band. One quantum eigenstate: Occupation numbers n_i vs. rescaled exitation energies $\epsilon_i = \delta_i$.
Left: 5th state, $J/J_c \approx 0.15$, $T_{FD} = 0.15\delta$, $\delta E = 0.97\delta$, entropy $S = 0.49$.
Right: 100th state, $J/J_c \approx 1.5$, $T_{FD} = 0.20\delta$, $\delta E = 1.19\delta$, $S = 8.41$.
Full curves: Fermi-Dirac thermal distribution with given temperature T.

G.Benenti *et al.* (2001)

Dynamical thermalization of QC

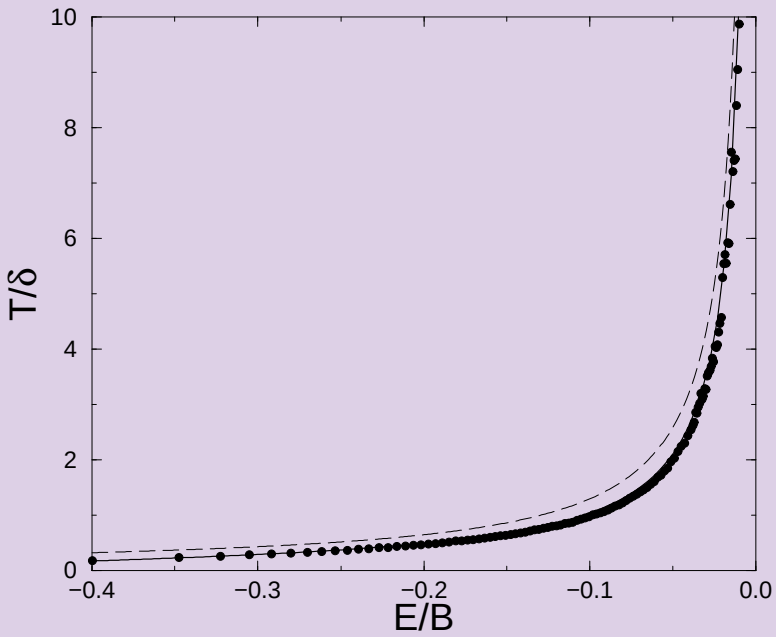

ψ_k register state; ϕ_m eigenstate;
$W_{km} = |<\psi_k|\phi_m>|^2$, entropy
$S_q = -\sum_k W_{km} \log_2 W_{km}$, central band,
occupation number
$n_i(m) = \sum_{k=1}^{N_B} W_{km} \langle\psi_k|\hat{n}_i|\psi_k\rangle$, with
$\langle\psi_k|\hat{n}_i|\psi_k\rangle = 1; 0$ for spin up/down in state i;
$\sum_{i=1}^{n} n_i(m) = [n/2]$, $\sum_{i=1}^{n} n_i(m)\delta_i = E_m^{'}$
(Left: $n = 16, J = 0.3\delta$, $B \approx n\delta/2$ is band width, 2 disorder realisations)

Fermi-Dirac distribution $n_i^{FD} = 1/[\exp(\beta(\delta_i + \delta/2 - \mu)) + 1]$, $\beta = 1/T_{FD}$;
$\sum_i n_i^{FD} = [n/2]$ and T_{FD} is the only fitting parameter
$E(T_{can}) = [\sum_m E_m \exp(-E_m/T_{can})]/\sum_m \exp(-E_m/T_{can})$,
$1/T_{th} = dS_{th}/dE = d\ln\rho/dE$, density of states $\rho \approx (1/\sqrt{2\pi}\sigma)\exp(-E^2/\sigma^2)$,
$T_{th} \sim -\sigma^2/E$ (previous right fig: $T_{FD} = 0.20\delta$, $T_{can} = 0.19\delta$)

G.Benenti *et al.* (2001)

Elementary quantum gates

PHYSICAL REVIEW A VOLUME 54, NUMBER 1 JULY 1996

Quantum networks for elementary arithmetic operations

Vlatko Vedral,* Adriano Barenco, and Artur Ekert
Clarendon Laboratory, Department of Physics, University of Oxford, Oxford OX1 3PU, United Kingdom
(Received 3 November 1995)

Quantum computers require quantum arithmetic. We provide an explicit construction of quantum networks effecting basic arithmetic operations: from addition to modular exponentiation. Quantum modular exponentiation seems to be the most difficult (time and space consuming) part of Shor's quantum factorizing algorithm. We show that the auxiliary memory required to perform this operation in a reversible way grows linearly with the size of the number to be factorized. [S1050-2947(96)05707-1]

PACS number(s): 03.65.Ca, 07.05.Bx, 89.80.+h

any unitary matrix of size $N = 2^n$ can be represented as a sequence of one-qubit and two-qubit gates (universal quantum gates)

Examples: quantum Fourier transform QFT ($N_g = n(n+1)/2$); Shor algorithm for number factorization ($N_g = O(n^3)$ vs. classical $N_g = O(\exp(n^{1/3}))$; Grover search algorithm ($N_g = O(\sqrt{N})$; quantum chaos evolution $N_g = O(n^2)$ with measurement information extraction problem

Elementary quantum gates

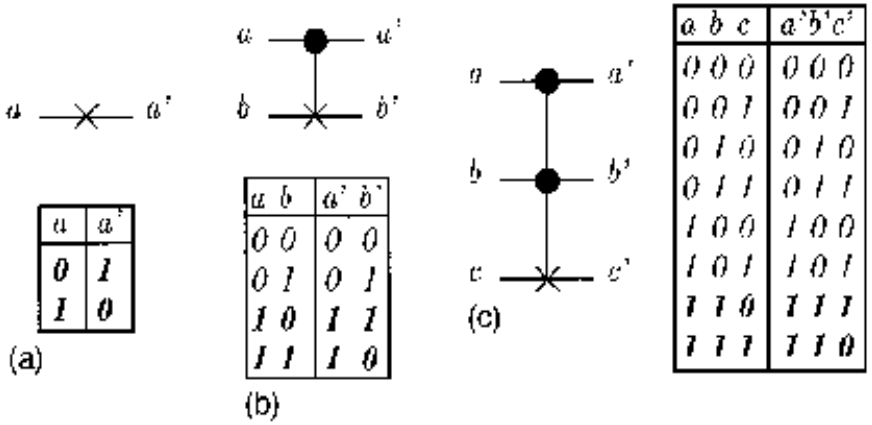

a	a'
0	1
1	0

a	b	a'	b'
0	0	0	0
0	1	0	1
1	0	1	1
1	1	1	0

a	b	c	a'	b'	c'
0	0	0	0	0	0
0	0	1	0	0	1
0	1	0	0	1	0
0	1	1	0	1	1
1	0	0	1	0	0
1	0	1	1	0	1
1	1	0	1	1	1
1	1	1	1	1	0

FIG. 1. Truth tables and graphical representations of the elementary quantum gates used for the construction of more complicated quantum networks. The control qubits are graphically represented by a dot, the target qubits by a cross. (a) NOT operation. (b) control-NOT. This gate can be seen as a "copy operation" in the sense that a target qubit (b) initially in the state 0 will be after the action of the gate in the same state as the control qubit. (c) Toffoli gate. This gate can also be seen as a control-control-NOT: the target bit (c) undergoes a NOT operation only when the two controls (a and b) are in state 1.

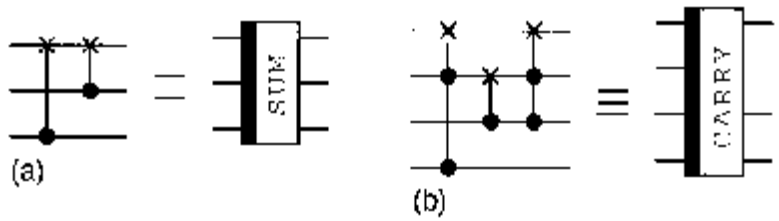

FIG. 3. Basic carry and sum operations for the plain addition network. (a) the carry operation (note that the carry operation perturbs the state of the qubit b). (b) the sum operation.

Elementary quantum gates

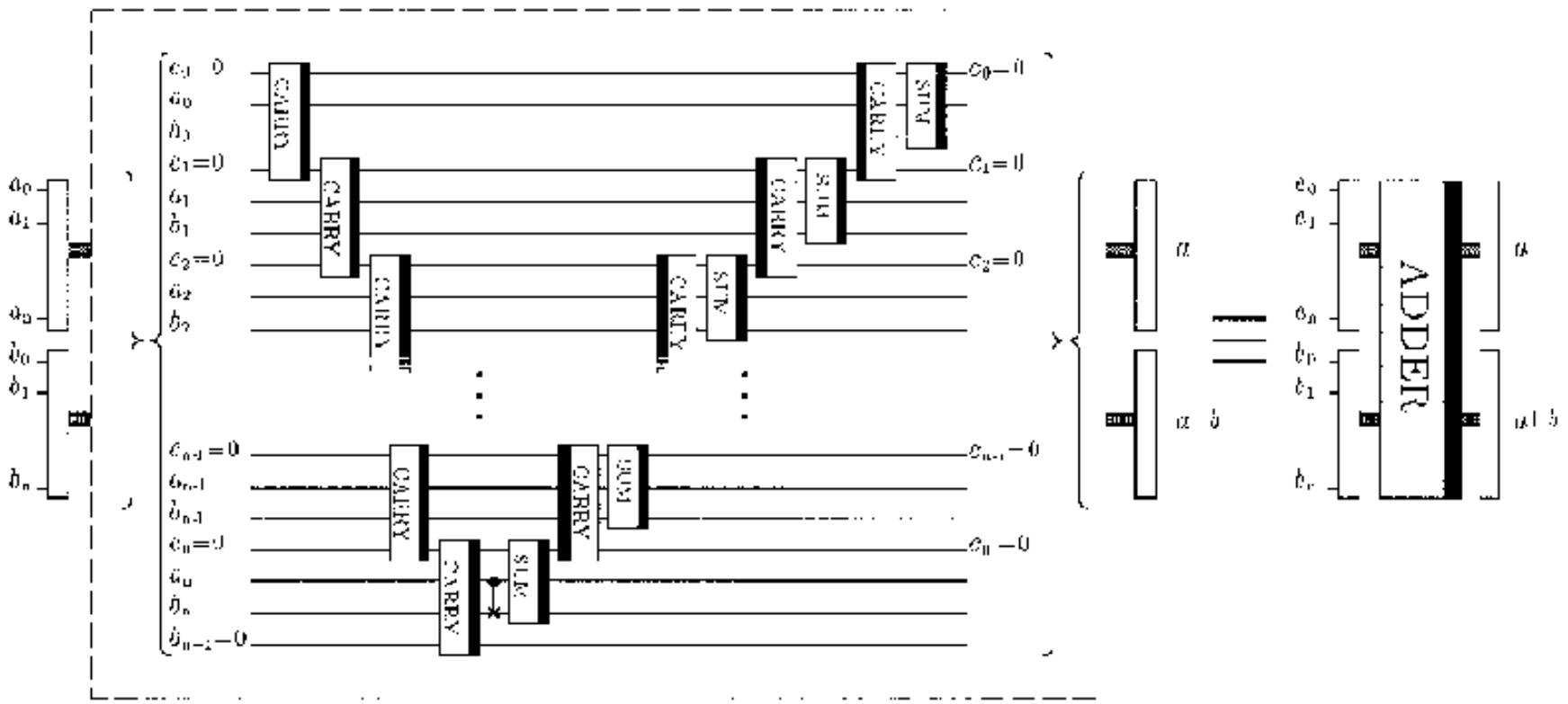

FIG. 2. Plain adder network. In the first step, all the carries are calculated until the last carry gives the most significant digit of the result. Then all these operations apart from the last one are undone in reverse order, and the sum of the digits is performed correspondingly. Note the position of a thick black bar on the right- or left-hand side of basic carry and sum networks. A network with a bar on the left side represents the reversed sequence of elementary gates embedded in the same network with the bar on the right side.

Quantum computing with imperfections

Accuracy measure of QC is fidelity: $f(t) = |<\psi(t)|\psi_\epsilon(t)>|^2$

Quantum algorithm: $|\psi(t)>= U^t\,|\psi(0)>$, elementary gates $U = U_{N_g} \cdot \ldots \cdot U_1$

Errors: $U_j \rightarrow U_j\, e^{i\delta H}$, $\delta H \sim \epsilon$

- Decoherence due to residual couplings of quantum computer to external bath: δH random and different at each j and t,

  e.g.: random phase fluctuations: $\delta\phi \in [-\epsilon, \epsilon]$ in phase-shift gates.
- Static imperfections in the quantum computer itself:

  δH (random but) constant at each j and t,

  e.g.: $\delta H = \sum_{j=0}^{n_q-1} \delta_j\, \sigma_j^{(z)} + 2\sum_{j=0}^{n_q-2} J_j\, \sigma_j^{(x)}\, \sigma_{j+1}^{(x)} \quad , \quad J_j, \delta_j \in [-\epsilon, \epsilon]$
- Non-unitary errors in quantum computation:

  $e^{i\delta H}$ is non-unitary ($\delta H \neq \delta H^\dagger$),
  density matrix and quantum trajectories approach

  Georgeot, DS (2001), Benenti *et al.* (2001), ..., Frahm *et al.* (2004), J.W.Lee, DS (2005)

Quantum algorithms of quantum maps

Since the Floquet operator is a composition of operators which are diagonal in the position and momentum space, it is easy implemented using the QFT F moving from one representation to another:

$$U = F^{+} \times e^{-i\alpha p^2} \times F e^{-i\beta x^p}$$

This allows to simulate one time step evolution of the system on a quantum computer in a polynomial time. The potential can be expanded in powrs and using repsentation $x = \sum_{j=0}^{n-1} a_j 2^j$ we have

$$e^{-i2\pi\gamma x^p} = \Pi_{j_1 \ldots j_p} e^{-i2\pi} a_{j_1} \cdots a_{j_p} 2^{j_1 + \ldots + j_p}$$

Quantum algorithm for Arnold cat map

$\bar{y} = y + x (mod 1)$
$\bar{x} = x + \bar{y} (mod 1)$ time inversion at $t = t_r$

Discretization on a grid $N \times N$ with $N = 2^{n_q}$ where n_q is number of qubits for register $|x_i>$ or $|y_j>$: $x_i = i/N$, $y_j = j/N, 0 \leq i,j \leq N-1$ (i,j are integers)

Initial classical distribution in the phase space (x,y) is coded in the initial wave function:

$\psi(t=0) = \sum_{i,j} a_{ij} |x_i> |y_j> |0>$

with $a_{i,j} = 0$ or $1/\sqrt{N_d}$ where $N_d = O(N^2)$ is the number of classical orbits; workspace register $|0>$ has $n_q - 1$ qubits

Quantum algorithm is based on modular additions (see e.g. V.Vegral, A.Barenco, A.E.Ekert Phys. Rev. A **54**, 147 (1996)), it uses $8n_q - 10$ C-NOT gates and $8n_q - 12$ C-C-NOT (Toffoli) gates.

In total one map iteration requires: $O(n_q)$ quantum gates versus $O(2^{2n_q})$ classical operations. The Hilbert space has $N_H = 2^{3n_q - 1}$ states.

Time reversal of Arnold cat map on QC

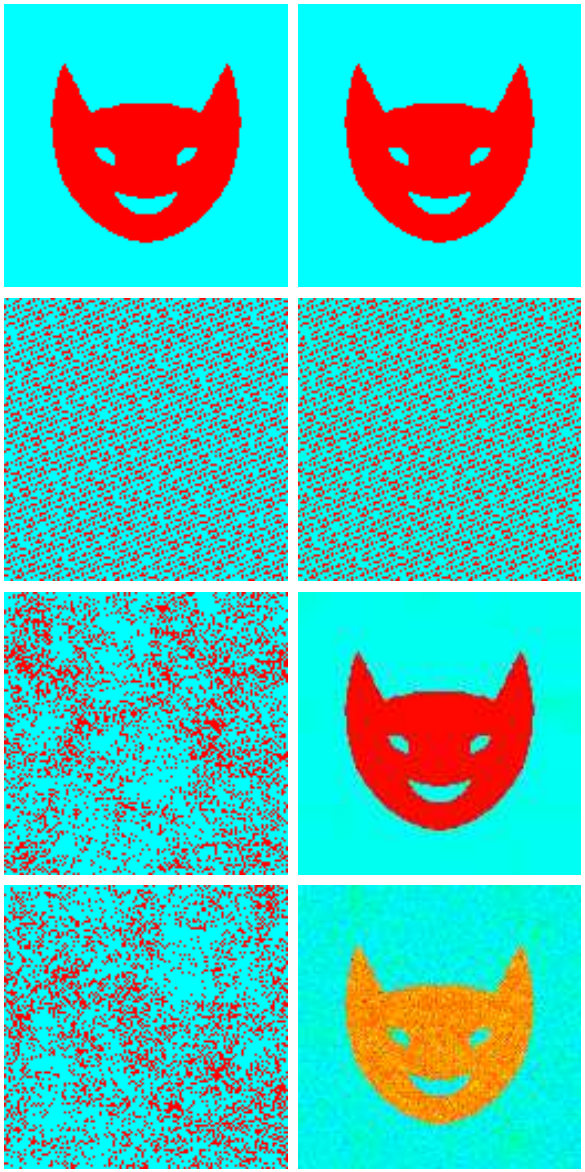

Dynamics of cat simulated on a classical (left) and quantum computer (right), on a 128×128 lattice. 1st row: $t = 0$; 2d row: time inversion at $t_r = 10$; 3d row: $t_{2r} = 20$; 4th row: $t_{2r} = 400$, with inversion at $t_r = 200$. Left: classical error of one cell size ($\epsilon = 1/128$) at $t = t_r$ only; right: quantum errors $\epsilon = 0.01$; color from blue to red is proportional to probability $|a_{ij}|^2$; $n_q = 7$. In total 20 qubits.

Time reversal of Arnold cat map on QC

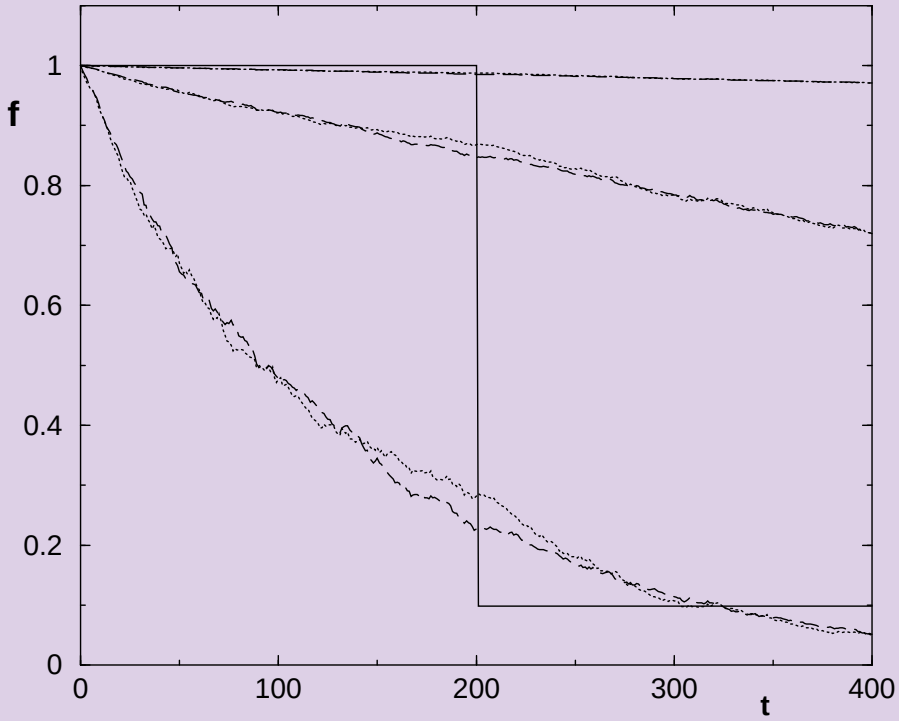

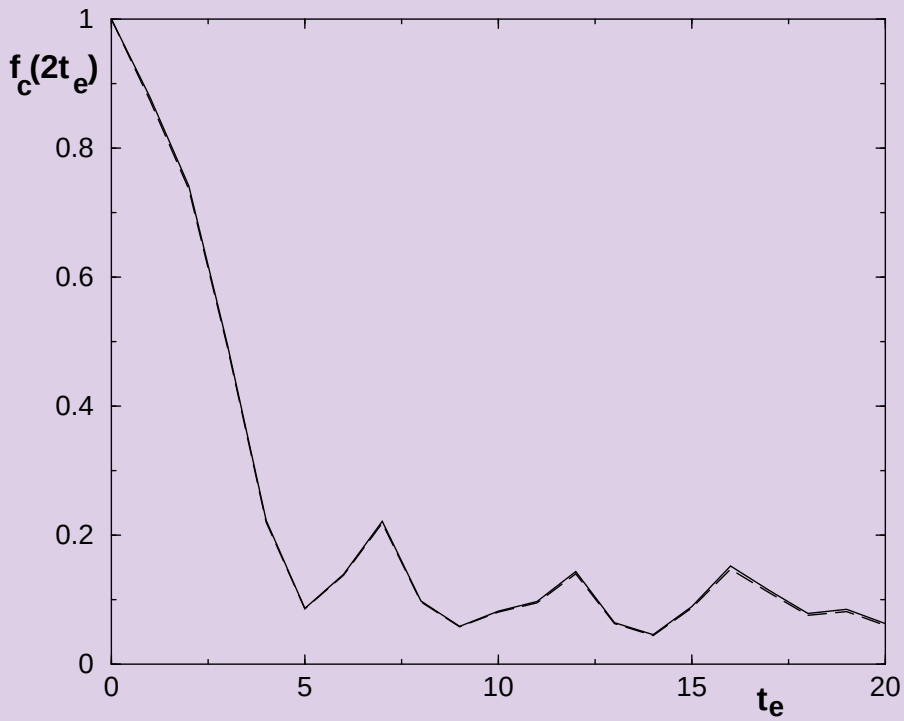

Left: Quantum fidelity f of Arnold-Schrödinger cat as a function of time t for quantum errors $\epsilon = 0.003, 0.01, 0.03$ (top to bottom). Initial state: cat and line $x = 1/2$. Full curve shows fidelity drop for minimal classical error done at $t = 200$. Fidelity time scale $t_f \approx 0.6/(\epsilon^2 n_q)$.

Rigth: Classical fidelity $f_c(2t_e)$ vs. time t_e for minimal classical error ($\epsilon = 1/128$) is made (full); dashed curve shows f_c obtained on a quantum computer with amplitude imperfections $\epsilon = 0.01$. Here $t_f \approx 1.4 \ln(1/\epsilon)$.

Time reversal of Arnold cat map on QC

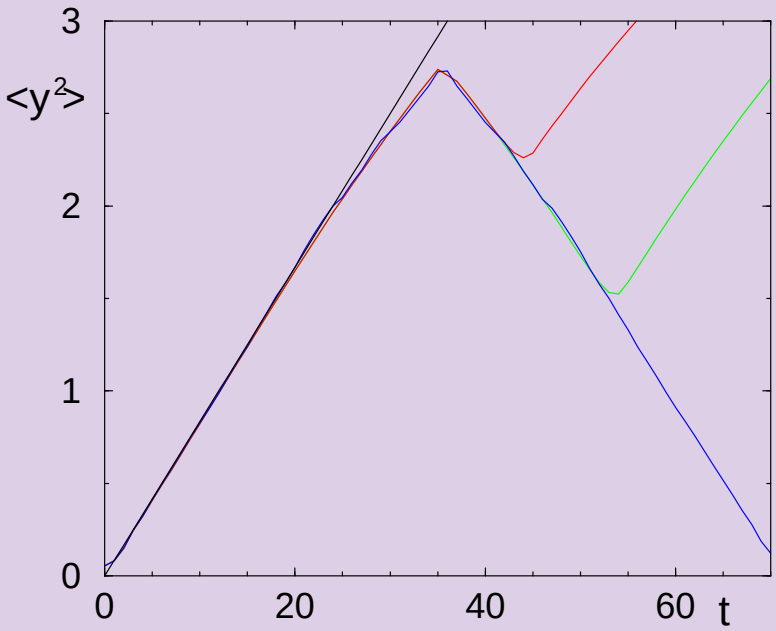

Map: $\bar{y} = y + x(modL)$; $\bar{x} = x + \bar{y}(mod1)$. Diffusive growth of $< y^2 >$ for the map at $L = 8$, simulated on a classical (Pentium III) and quantum ("Quantium I") computers. At $t = t_r = 35$ one inverts all velocities. For Pentium III inversion is done with precision $\epsilon = 10^{-4}$ and $\epsilon = 10^{-8}$; 10^6 orbits are simulated, initially distributed inside the demon image. For Quantium I, the computation is done with ($n_q = 26$ qubits)(blue line); each quantum gate operates with random noise rotation of amplitude $\epsilon = 0.01$. The black straight line shows the theoretical macroscopic diffusion with $D = 1/12$.

A quantum computer with 125 qubits can perform Boltzmann's demand for Avogadro's number of classical chaotic orbits.

Quantum sawtooth map on QC

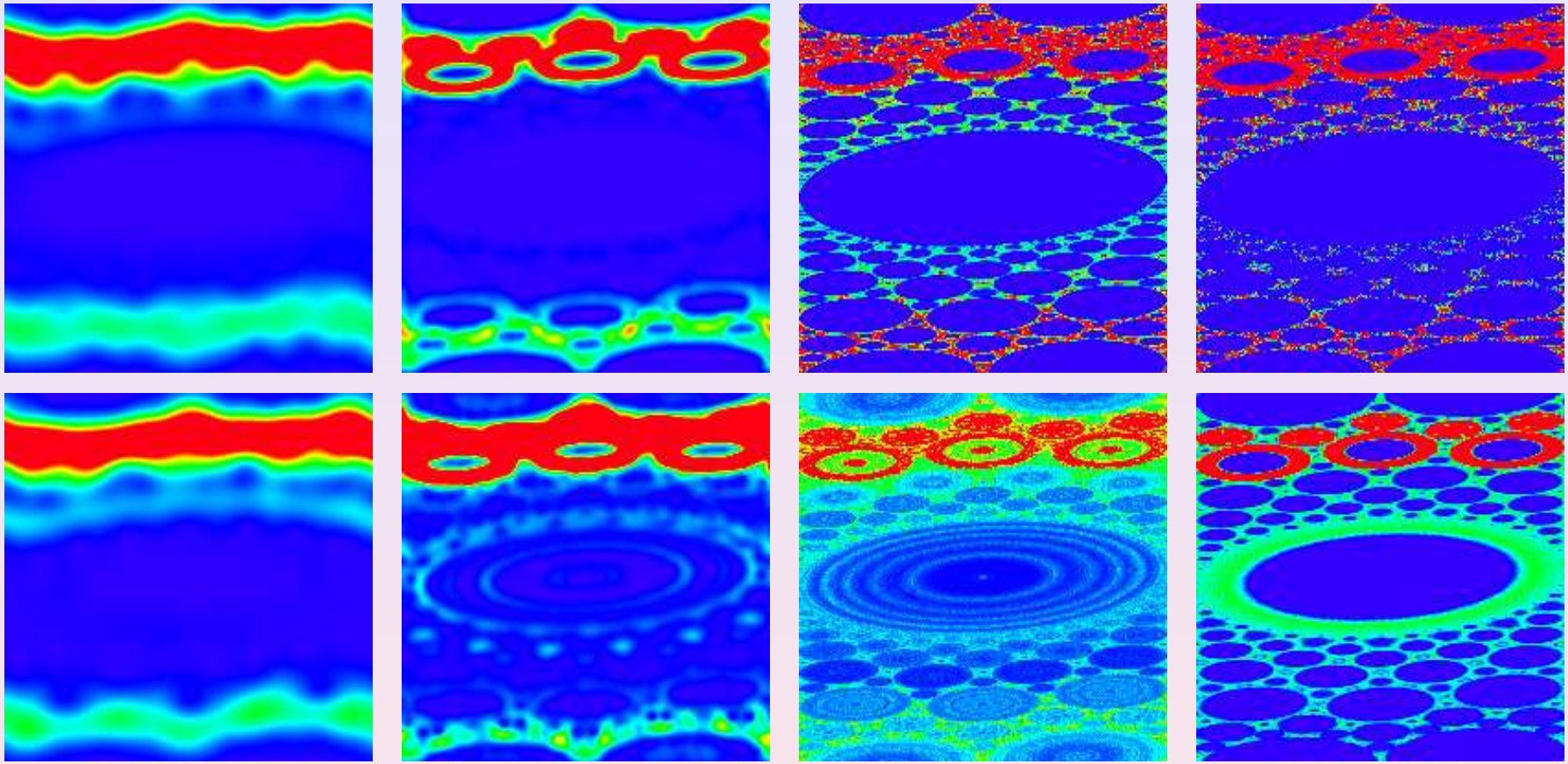

Map: $\overline{n} = n + k(\theta - \pi), \quad \overline{\theta} = \theta + T\overline{n}, mod(2\pi); K = kT = -0.1, \quad T = 2\pi/2^{n_q}$, number of gates $n_g = 3n_q^2 + n_q$, with swaps $n_g = O(n_q^{5/2})$ local gates; $t \approx 1000, J = 0$; color shows Husimi function density
Top row: $\epsilon = 0$; bottom row: $\epsilon \approx 0.5/n_q^3$; from left to right $n_q = 6; 9; 16$, right panels: classical map exact (top) and with round-off error 10^{-3}.

Hypersensitivity of QC eigenstates

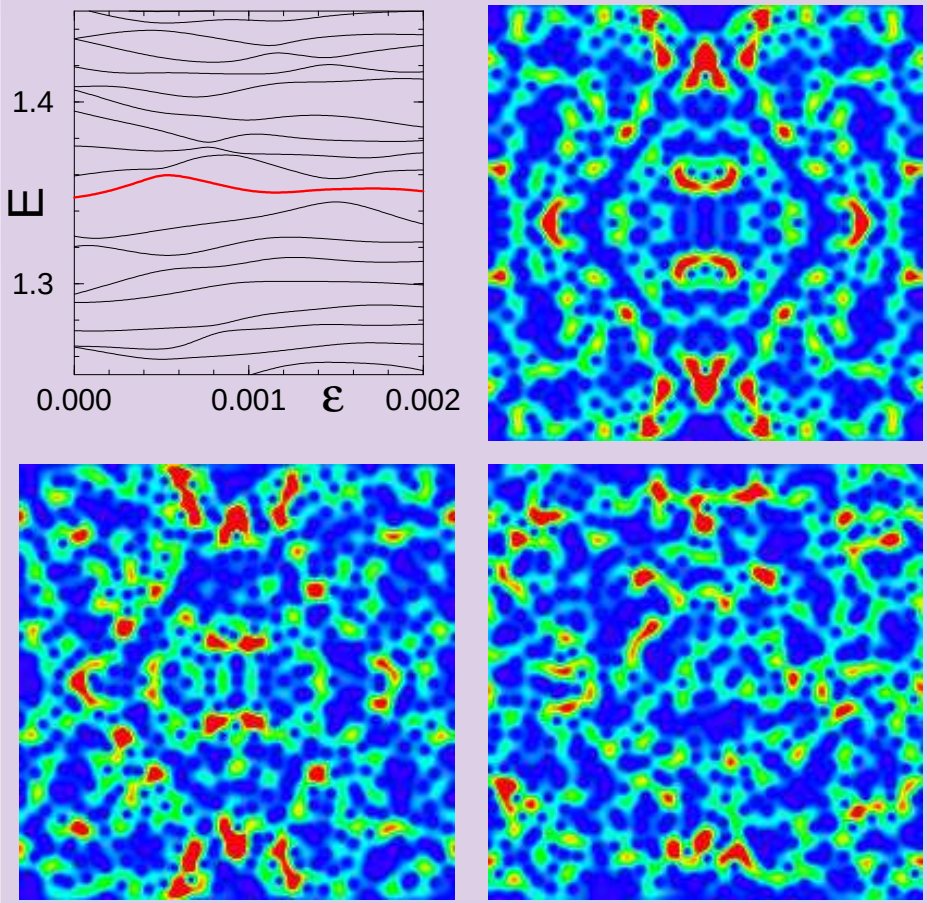

Variation of quasienergy (red curve) and corresponding eigenstate (shown by Husimi function) of unitary evolution operator of quantum sawtooth map with static imperfections strength ϵ. Here $\epsilon = 0,\ 4 \times 10^{-4},\ 10^{-3}$ (right top, left/right bottom); and $K = kT = \sqrt{2}, T = 2\pi/N,\ \ N = 2^{n_q}, J = 0, n_q = 9$. Mixing of levels takes place at critical interaction strength: $\epsilon_\chi \sim 1/\sqrt{N} \sim 2^{-n_q/2}$

Quantum sawtooth map: $\overline{\psi} = e^{-iT\hat{n}^2/4} e^{ik(\hat{\theta}-\pi)^2/2} e^{-iT\hat{n}^2/4} \psi = e^{-iE}\psi$

Quantum tent map

$$H(t) = Tp^2/2 + V(\theta)\sum \delta(t-n)$$

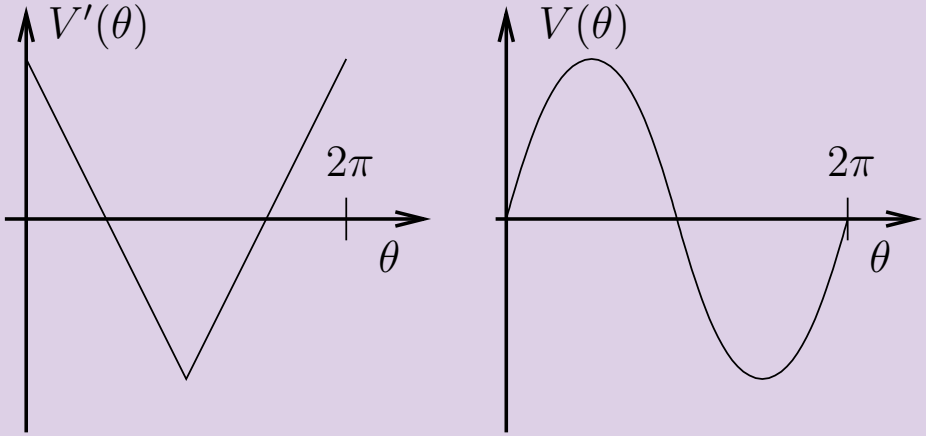

Classical map:

$p_{n+1} = p_n - V'(\theta_n)$

$\theta_{n+1} = \theta_n + T\, p_{n+1}$

Quantum map: $p = -i\partial/\partial\theta$

$|\psi(t+1)> = U|\psi(t)>$

$U = e^{-Tp^2/2}\, e^{-iV(\theta)}$

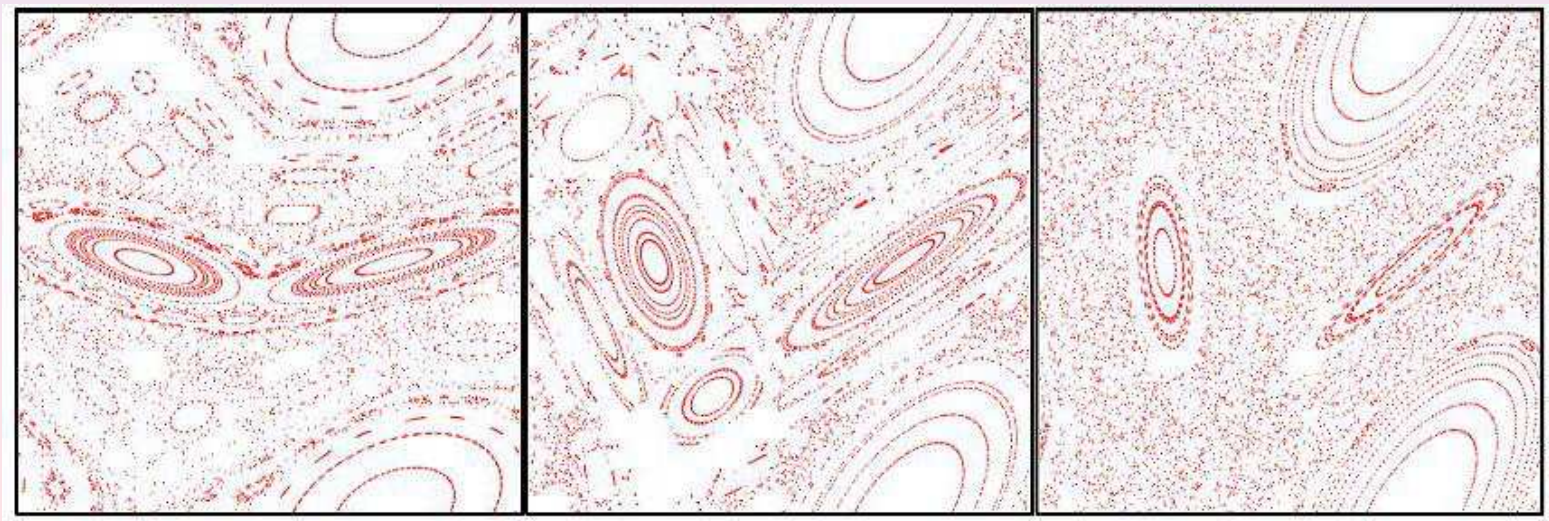

$T = 1, K = k = 0.53; 4/3; 1.7$

Quantum algorithm for quantum tent map

Quantum register identification: $|p> \equiv |\alpha_0>_0 |\alpha_1>_1 \ldots |\alpha_{nq-1}>_{nq-1}$.

$$p = \sum_{j=0}^{n_q-1} \alpha_j \, 2^j \ \in \ \{0, \ldots, N-1\}$$

$N = 2^{n_q}$ = dimension of Hilbert space; n_q = number of qubits; $\alpha_j \ \in \ \{0, 1\}$.

Quantum Fourier transform: $p \leftrightarrow \theta$ and $e^{-iTp^2/2} |p> = \prod_{j<k} \underbrace{e^{i(\cdots)\alpha_j\alpha_k}}_{B^{(2)}_{jk}(\cdots)} \prod_j \underbrace{e^{i(\cdots)\alpha_j}}_{B^{(1)}_j(\cdots)} |p>$.

with simple and controlled phase-shift:

$$B^{(1)}_j(\phi) = \begin{pmatrix} 1 & 0 \\ 0 & e^{i\phi} \end{pmatrix} \quad , \quad B^{(2)}_{jk}(\phi) = \begin{pmatrix} 1 & 0 & 0 & 0 \\ 0 & 1 & 0 & 0 \\ 0 & 0 & 1 & 0 \\ 0 & 0 & 0 & e^{i\phi} \end{pmatrix} .$$

Double controlled phase-shift: $B^{(3)}_{jkl}(\phi) = B^{(2)}_{jl}\left(\frac{\phi}{2}\right) B^{(2)}_{jk}\left(\frac{\phi}{2}\right) C^{(N)}_{kl} B^{(2)}_{jk}\left(-\frac{\phi}{2}\right) C^{(N)}_{kl}$.

Number of elementary gates: $n_g \approx 9\, n_q^2/2$

Quantum algorithm for quantum tent map

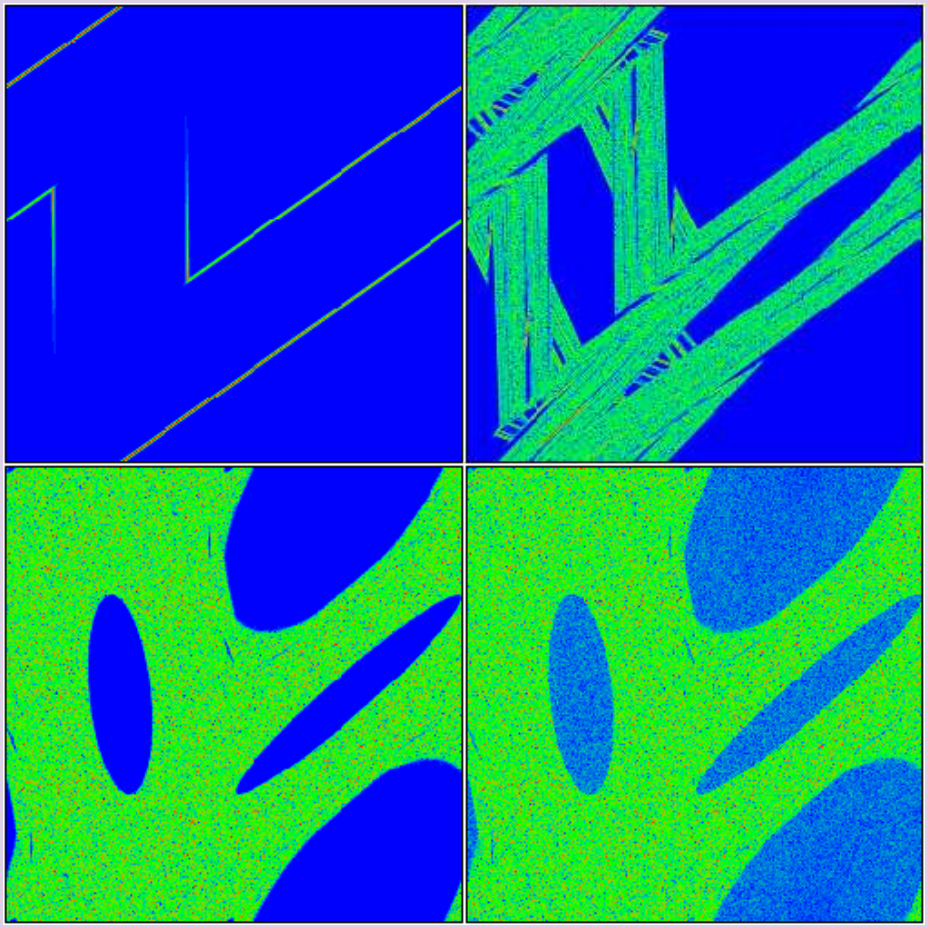

Husimi function: $t = 5, 15, 5625 (\epsilon = 0)$ and $t = 5625 (\epsilon = 7 \cdot 10^{-7})$; $K = 1.7$, $\hbar_{eff} = T = 2\pi/N$, $N = 2^{n_q}$, $n_q = 16$.

Poincaré section

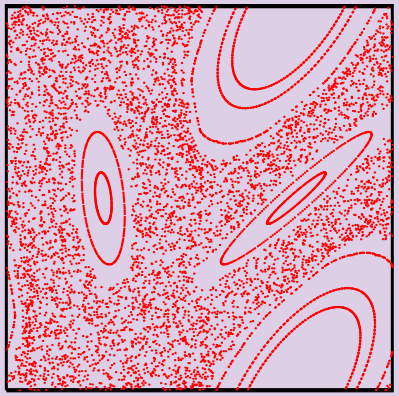

Fidelity decay with errors

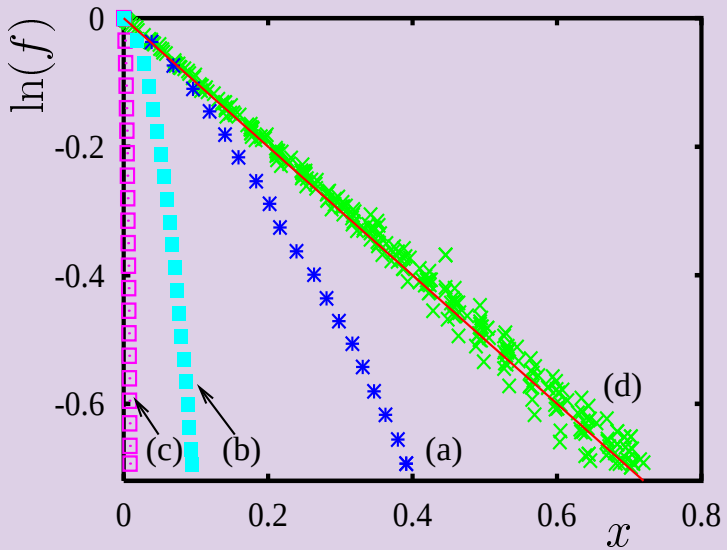

(static $x = t/t_c$ (a,b,c); random $x = t/t_r$ (d))

Random matrix theory for fidelity decay

Fidelity with average initial state: $f(t) = \left| \frac{1}{N} \mathrm{Tr} \left(U^{-t} \left(U\, e^{i\delta H_{eff}} \right)^t \right) \right|^2$

Regime $(1-f) \ll 1$: $f(t) \approx 1 - \frac{t}{t_c} - \frac{2}{t_c} \sum_{\tau=1}^{t-1} (t-\tau)\, C(\tau)$

with: $1/t_c = \mathrm{Tr}\left({\delta H_{eff}}^2 \right)/N$, $C(\tau) = \frac{t_c}{N} \mathrm{Tr}\Big(\underbrace{U^{-\tau}\, \delta H_{eff}\, U^{\tau}}_{\delta H_{eff}(\tau)}\, \delta H_{eff} \Big)$

$U \in$ COE (CUE) $\Rightarrow$ Scaling law:
$-\langle \ln f(t) \rangle_U \approx \frac{N}{t_c} \chi\left(\frac{t}{N}\right)$, $\chi(s) = s + \frac{2}{\beta} s^2 - 2 \int_0^s d\tilde{\tau}\, (s-\tilde{\tau})\, b_2(\tilde{\tau})$.

with the "two-level form factor": $b_2(\tilde{\tau})$.

Scaling analysis of fidelity decay

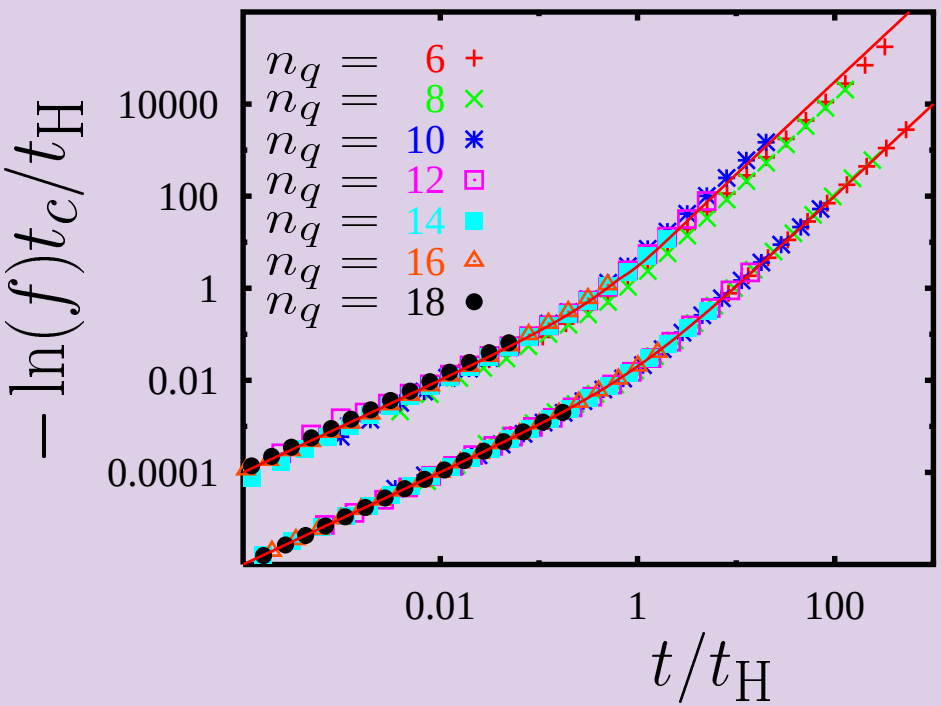

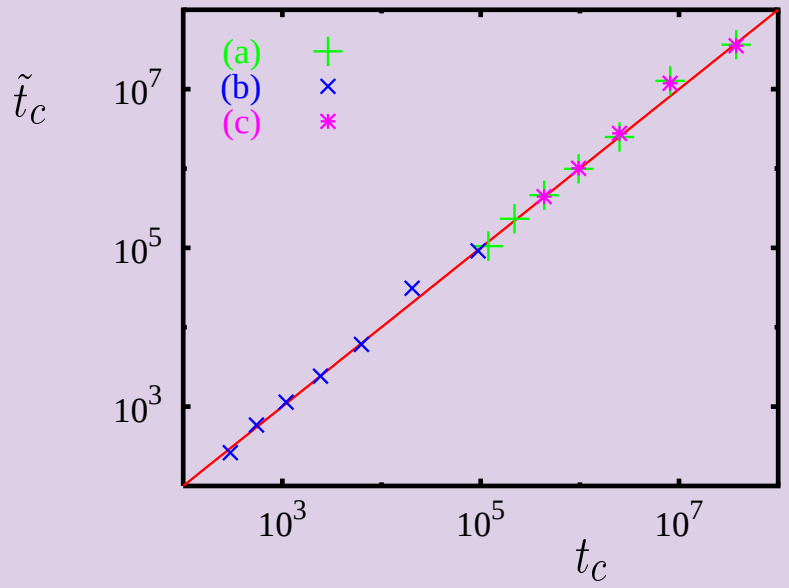

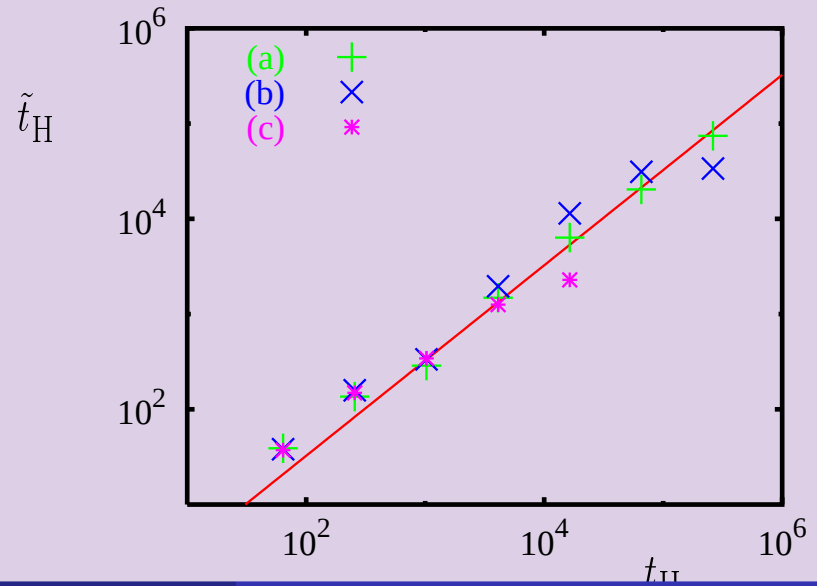

Upper curve: with theoretical values:
$t_H = 2^{n_q}$ and $t_c = 1/(\epsilon^2 n_q n_g^2)$

Lower curve: with fit values $\tilde{t}_c$ and $\tilde{t}_H$
from: $-\ln(f(t)) = \frac{t}{\tilde{t}_c} + \frac{t^2}{\tilde{t}_c \tilde{t}_H}$ $\quad (\tilde{t}_H \approx t_H/3)$

Cory group NMR QC of quantum sawtooth map

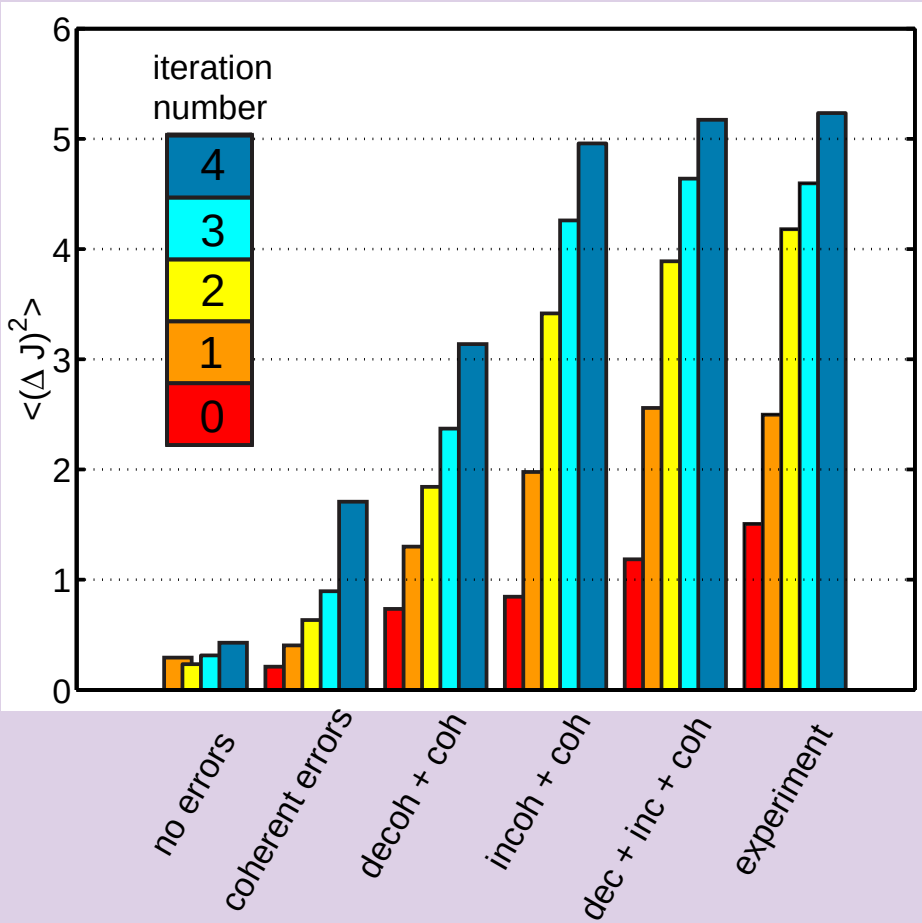

The second moment of the probability distribution determined from numerical simulations of the experiment including the error models discussed in the paper, compared to the ideal data and the experimental data. This plot demonstrates the relative importance of the individual noise mechanisms as they contribute to the experimentally observed delocalization process. As more errors are included in numerical simulations, the system shows stronger delocalization and more closely emulates the experimental data.

* 3 qubit QIP based on liquid state NMR: Cory *et al.* PRA **74**, 062317 (2006)
* Map parameters are $k = 0.27, K = kT = 1.5, (T = 5.55)$, diffusion rate $D = \pi^2 k^2/3 = 0.24$: regime of perturbative localization.

Synchronization of superconducting qubits

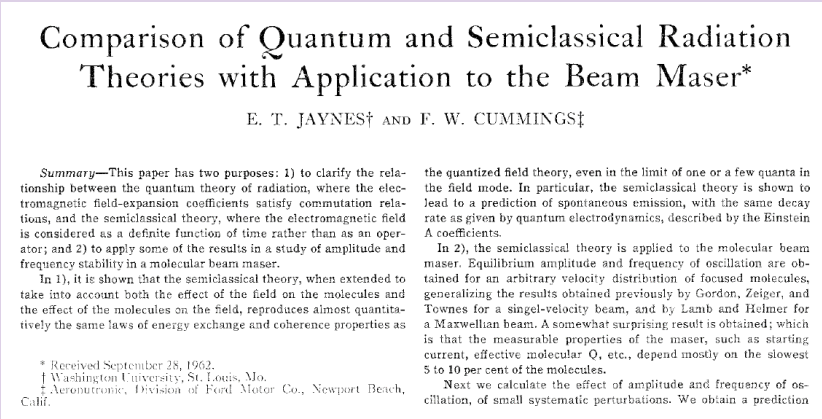

Comparison of Quantum and Semiclassical Radiation Theories with Application to the Beam Maser*

E. T. JAYNES† AND F. W. CUMMINGS‡

Summary—This paper has two purposes: 1) to clarify the relationship between the quantum theory of radiation, where the electromagnetic field-expansion coefficients satisfy commutation relations, and the semiclassical theory, where the electromagnetic field is considered as a definite function of time rather than as an operator; and 2) to apply some of the results in a study of amplitude and frequency stability in a molecular beam maser.

In 1), it is shown that the semiclassical theory, when extended to take into account both the effect of the field on the molecules and the effect of the molecules on the field, reproduces almost quantitatively the same laws of energy exchange and coherence properties as the quantized field theory, even in the limit of one or a few quanta in the field mode. In particular, the semiclassical theory is shown to lead to a prediction of spontaneous emission, with the same decay rate as given by quantum electrodynamics, described by the Einstein A coefficients.

In 2), the semiclassical theory is applied to the molecular beam maser. Equilibrium amplitude and frequency of oscillation are obtained for an arbitrary velocity distribution of focused molecules, generalizing the results obtained previously by Gordon, Zeiger, and Townes for a singel-velocity beam, and by Lamb and Helmer for a Maxwellian beam. A somewhat surprising result is obtained; which is that the measurable properties of the maser, such as starting current, effective molecular Q, etc., depend mostly on the slowest 5 to 10 per cent of the molecules.

Next we calculate the effect of amplitude and frequency of oscillation, of small systematic perturbations. We obtain a prediction

* Received September 28, 1962.
† Washington University, St. Louis, Mo.
‡ Aeronutronic, Division of Ford Motor Co., Newport Beach, Calif.

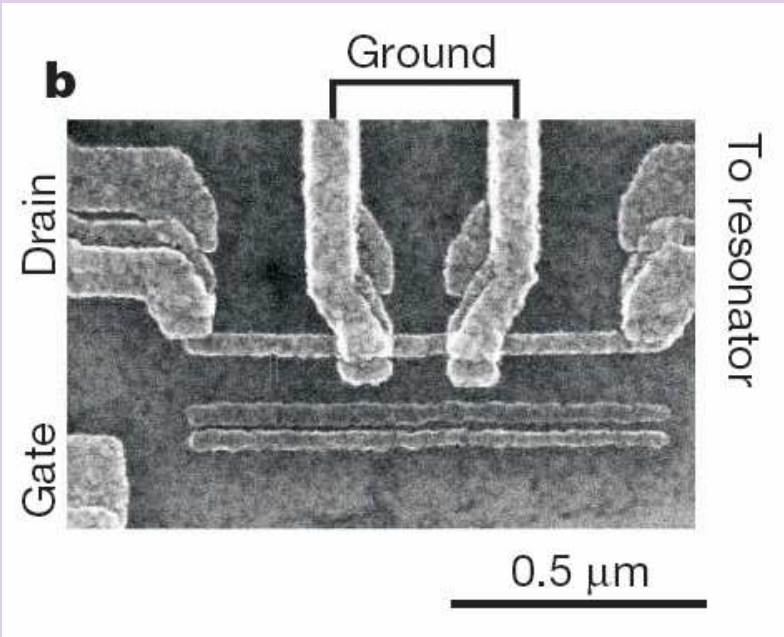

- (1963) Jaynes-Cummings model (Proc. IEEE)
- Hamiltonian:
  qubit coupled to resonator
  $\hat{H} = \hbar\omega_0\hat{n} - \hbar\Omega\sigma_x/2$
  $+g\hbar\omega_0(\hat{a}+\hat{a}^\dagger)\sigma_z + f\cos\omega t\,(\hat{a}+\hat{a}^\dagger)$
- Master equation for the density matrix:
  $\dot{\hat{\rho}} = -i[\hat{H},\hat{\rho}]/\hbar$
  $+\lambda(\hat{a}\hat{\rho}\hat{a}^\dagger - \hat{a}^\dagger\hat{a}\hat{\rho}/2 - \hat{\rho}\hat{a}^\dagger\hat{a}/2)$
- Quality factor: $Q = \omega_0/\lambda \sim 100$
  Zhirov, DS, PRL 100, 014101 (2008)
- Single artificial-atom lasing
  O. Astafiev *et al.* Nature 449, 588 (2007)

Synchronization and bistability of qubit

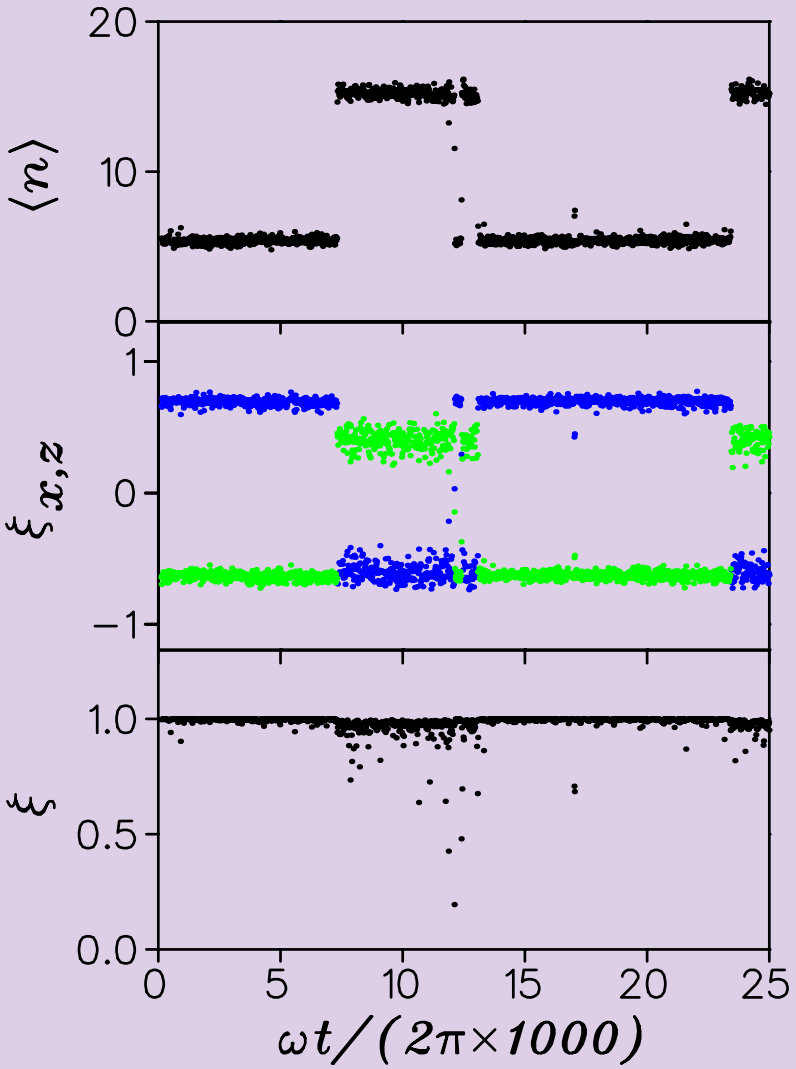

- Fig.1: Bistability of qubit coupled to a driven oscillator with jumps between two metastable states. Top panel shows average oscillator level number $\langle n \rangle$ as a function of time t at stroboscopic integer values $\omega t/2\pi$; middle panel shows the qubit polarization vector components ξ_x (blue) and ξ_z (green) at the same moments of time; the bottom panel shows the degree of qubit polarization ξ. Here the system parameters are $\lambda/\omega_0 = 0.02$, $\omega/\omega_0 = 1.01$, $\Omega/\omega_0 = 1.2$, $f = \hbar\lambda\sqrt{n_p}$, $n_p = 20$ and $g = 0.04$.

Dynamics and bistability of qubit

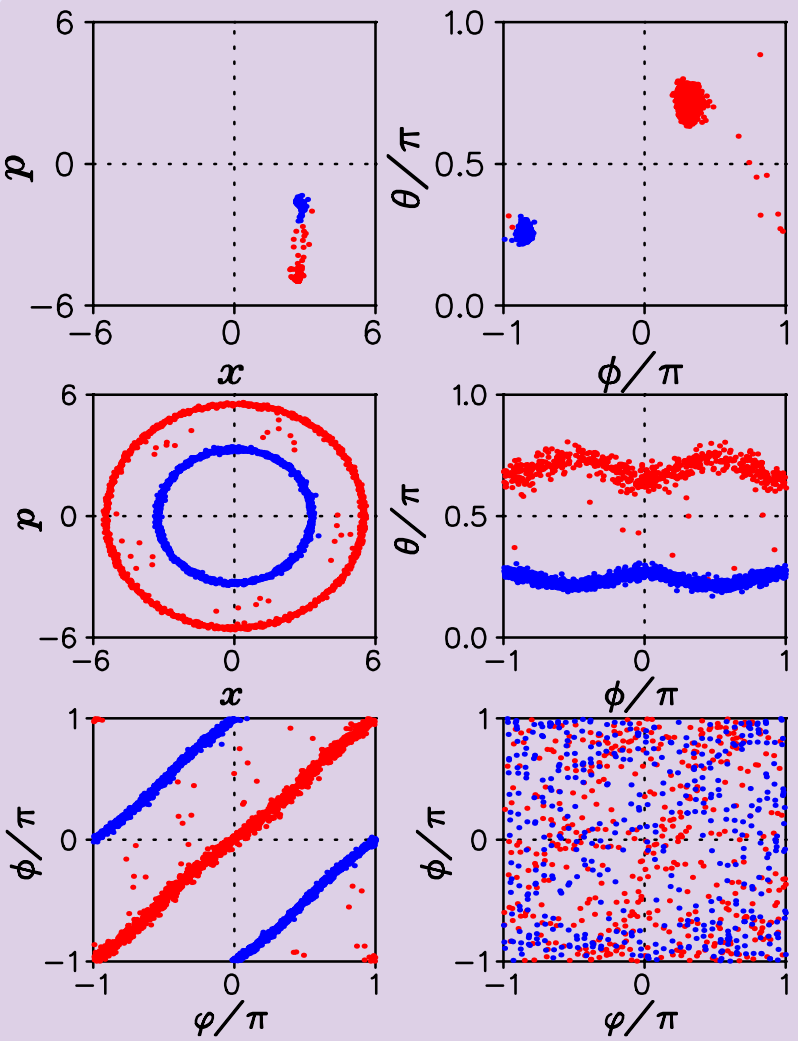

- Fig.2: Top panels: the Poincaré section taken at integer values of $\omega t/2\pi$ for oscillator with $x = \langle(\hat{a} + \hat{a}^\dagger)/\sqrt{2}\rangle$, $p = \langle(\hat{a} - \hat{a}^\dagger)/\sqrt{2}i\rangle$ (left) and for qubit polarization with polarization angles (θ, ϕ) defined in text (right). Middle panels: same quantities shown at irrational moments of $\omega t/2\pi$. Bottom panels: qubit phase ϕ *vs.* oscillator phase φ ($p/x = -\tan\varphi$) at time moments as in middle panels for $g = 0.04$ (left) and $g = 0.004$ (right). Other parameters and the time interval are as in Fig.1. The color of points is blue for $\xi_x > 0$ and red for $\xi_x < 0$.

Macroscopic detector of qubit state

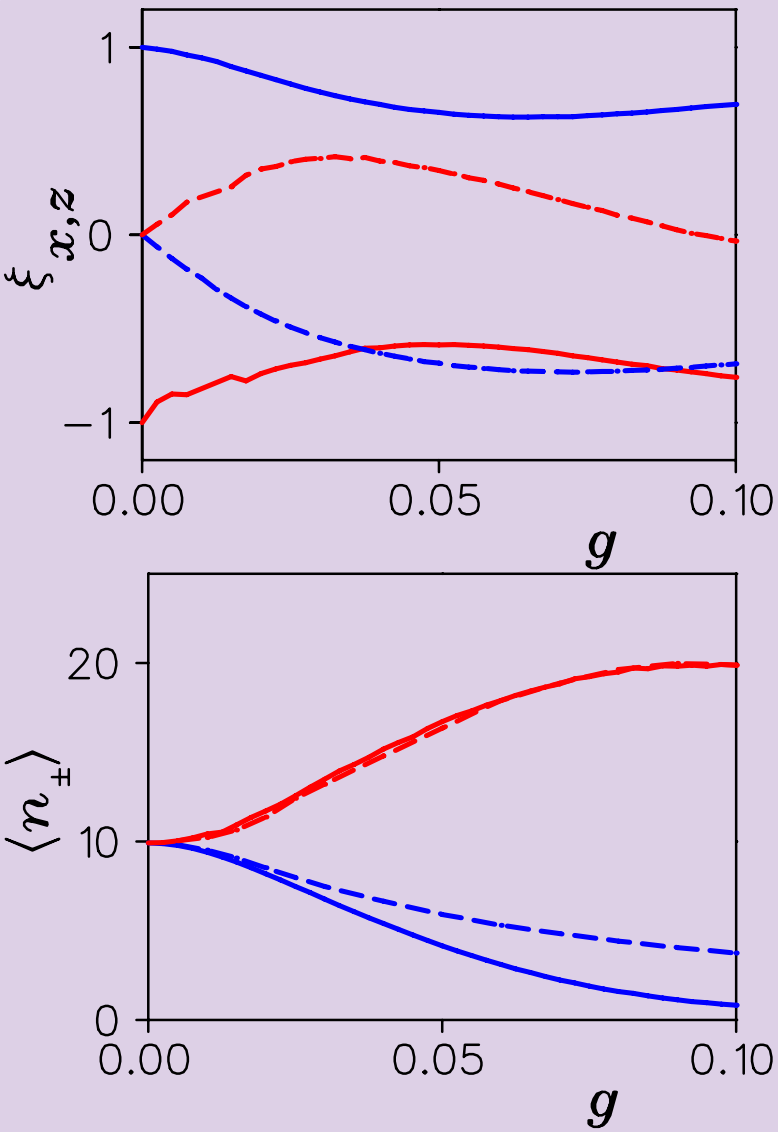

- Fig.3: Top panel: dependence of average qubit polarization components ξ_x and ξ_z (full and dashed curves) on g, averaging is done over stroboscopic times (see Fig.1) in the interval $100 \leq \omega t/2\pi \leq 2 \times 10^4$; color is fixed as in Fig.2. Bottom panel: dependence of average level of oscillator in two metastable states on coupling g, color is fixed by ξ_x sign on right panel (red for large n_+ and blue for small n_-); average is done over the quantum state and stroboscopic times as in the top panel; dashed curves show theory dependence (see text). Two QT are used with initial value $\xi_x = \pm 1$. All parameters are as in Fig.1 except g.

Macroscopic detector of qubit state

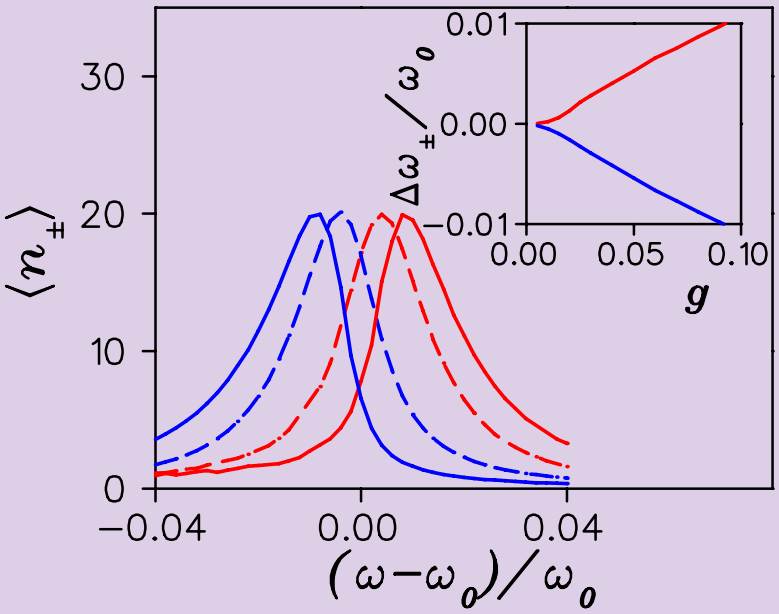

- Fig.4: Dependence of average level $n_\pm$ of oscillator in two metastable states on the driving frequency ω (average and color choice are the same as in right panel of Fig.3); coupling is $g = 0.04$ and $g = 0.08$ (dashed and full curves). Inset shows the variation of position of maximum at $\omega = \omega_\pm$ with coupling strength g, $\Delta\omega_\pm = \omega_\pm - \omega_0$. Other parameters are as in Fig.1.

Theoretical estimates: the shift $\Delta\omega_\pm$ explains two states $n_\pm$ of driven oscillator well described by $n_\pm = n_p\lambda^2/(4(\omega - \omega_0 - \Delta\omega_\pm)^2 + \lambda^2)]$ (see dashed curves in Fig.3 bottom traced with numerical values of $\Delta\omega_\pm$ from Fig.4 inset). To estimate $\Delta\omega_\pm$ we note that the frequency of effective Rabi oscillations between quasi-degenerate levels is $\Omega_R \approx g\omega_0\sqrt{n_\pm + 1}$ (JC-model) that gives $\Delta\omega_\pm \approx d\Omega_R/dn \approx \pm g\omega_0/2\sqrt{n_\pm + 1}$ in a good agreement with data.

Macroscopic quantum tunneling between qubit states

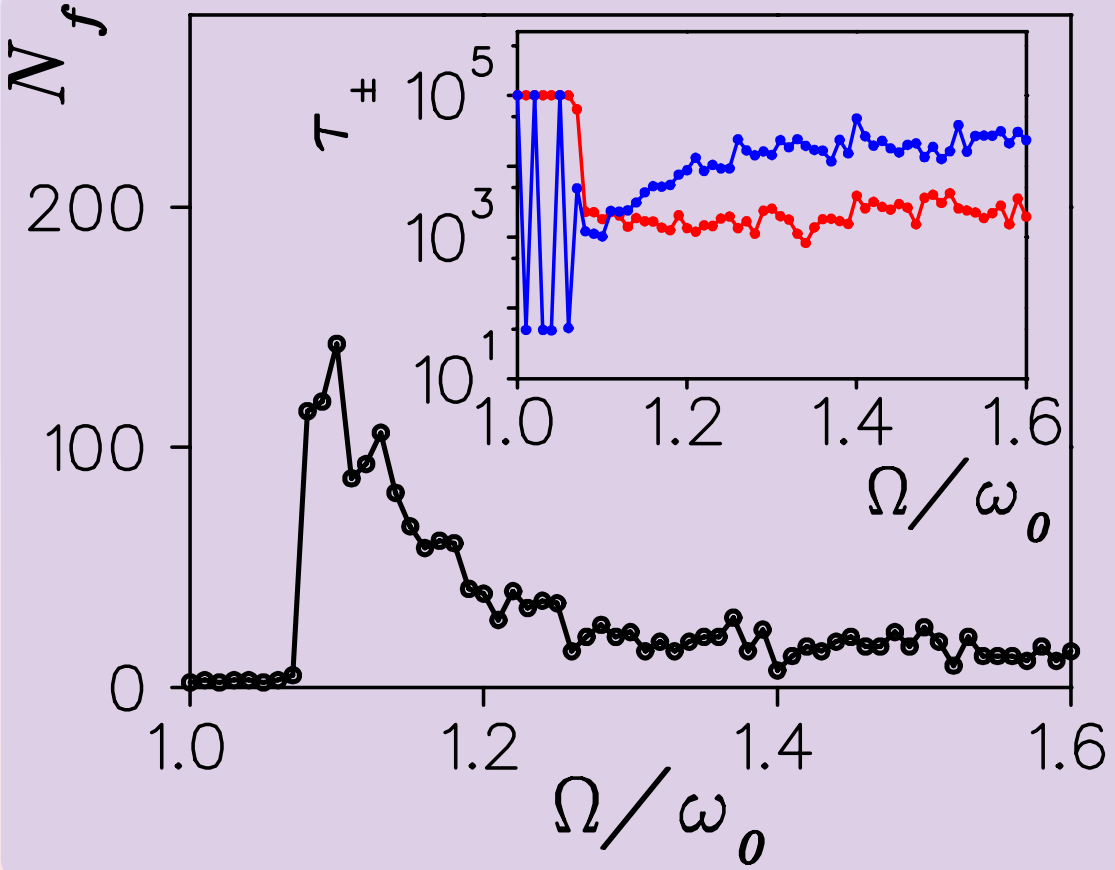

- Fig.5: Dependence of number of transitions N_f between metastable states on rescaled qubit frequency Ω/ω_0 for parameters of Fig.1; N_f are computed along 2 QT of length 10^5 driving periods. Inset shows life time dependence on Ω/ω_0 for two metastable states (τ_+ for red, τ_- for blue, $\tau_\pm$ are given in number of driving periods; color choice is as in Figs.2,3)

Radiation spectrum of qubit

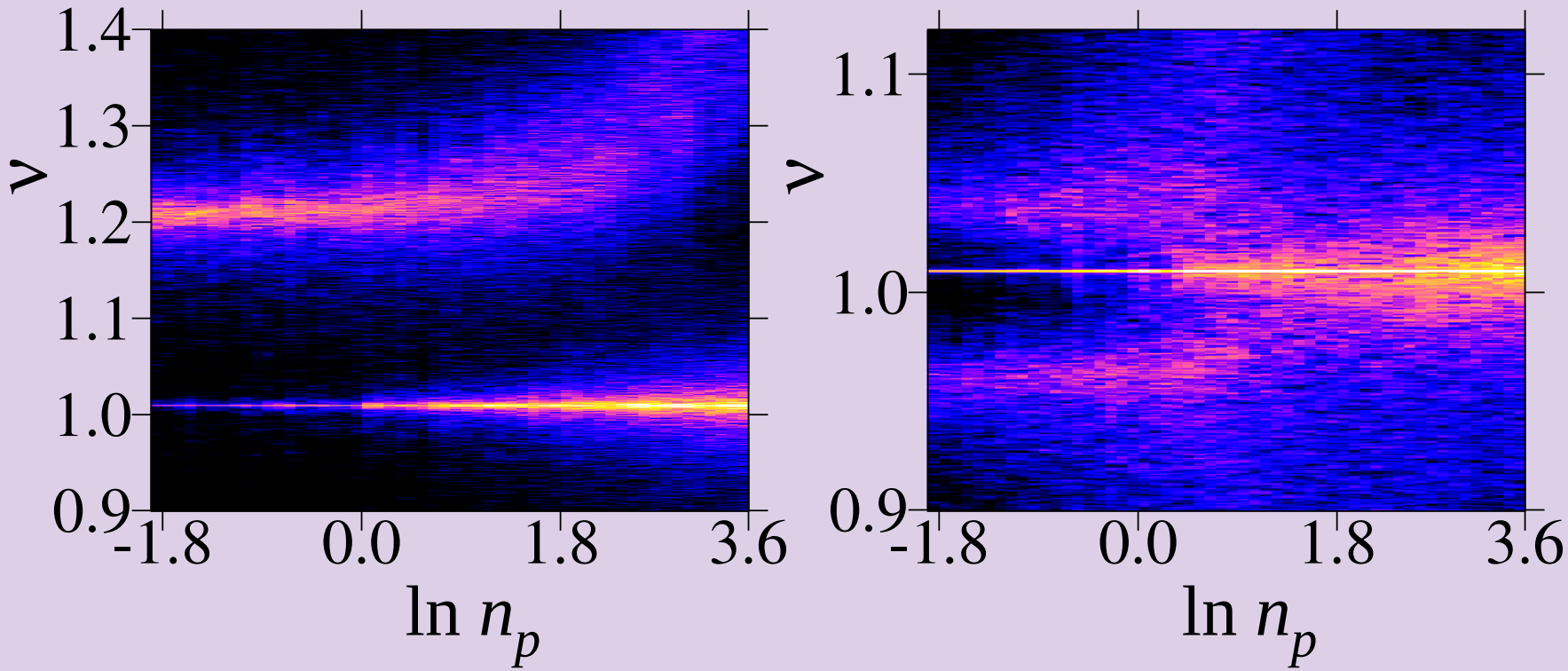

Fig.6: Spectral density $S(\nu)$ of qubit radiation $\xi_z(t)$ as function of driving power n_p in presence of phase noise in ϕ with diffusion rate $\eta = 0.004\omega_0$. Left: $\Omega/\omega_0 = 1.2$; right: $\Omega/\omega_0 = 1$. Other parameters are as in Fig.1. Color shows $S(\nu)$ in logarithmic scale (white/black for maximal/zero), ν is given in units of ω_0.

References:

L3.1. E.P.Wigner, *Characteristic vectors of bordered matrices with infinite dimensions*, Ann. Math. **62**, 548 (1955); *Characteristic vectors of bordered matrices of infinite dimensions II*, Ann. Math. **65**, 203 (1957)

L3.2. S.Åberg, *Onset of chaos in rapidly rotating nuclei*, Phys. Rev. Lett. **64**, 3119 (1990); *Quantum choas and rotational damping*, Prog. Part. Nucl. Phys. **28**, 11 (1992)

L3.3. D.L.Shepelyansky, O.P.Sushkov, *Few interacting particles in a random potential*, Europhys. Lett. **37**, 121 (1997)

L3.4. Ph.Jacquod and D.L.Shepelyansky, *Emergence of quantum chaos in finite interacting Fermi systems*, Phys. Rev. Lett. **79**, 1837 (1997)

L3.5. B.Georgeot and D.L.Shepelyansky, *Breit-Wigner width and inverse participation ratio in finite interacting Fermi systems*, Phys. Rev. Lett. **79**, 4365 (1997)

L3.6. K.Ahnert and A.Pikovsky, *Compactons and chaos in strongly nonlinear lattices* , Phys. Rev. E **79**, 026209 (2009)

L3.7. O.V.Zhirov, A.S.Pikovsky and D.L.Shepelyansky, *Quantum vacuum of strongly nonlinear lattices*, Phys. Rev. E **83**, 016202 (2011)

L3.8. B.Georgeot and D.L.Shepelyansky, *Quantum chaos border for quantum computing*, Phys. Rev. E **62**, 3504 (2000); *Emergence of quantum chaos in the quantum computer core and how to manage it*, Phys. Rev. E **62**, 6366 (2000)

L3.9. G.Benenti, G.Casati and D.L.Shepelyansky, *Emergence of Fermi-Dirac thermalization in the quantum computer core*, Eur. Phys. J. D **17**, 265 (2001)

References (continued):

L3.10. B.Georgeot and D.L.Shepelyansky, *Exponential gain in quantum computing of quantum chaos and localization*, Phys. Rev. Lett. **86**, 2890 (2001)

L3.11. B.Georgeot and D.L.Shepelyansky, *Stable quantum computation of unstable classical chaos*, Phys. Rev. Lett. **86**, 5393 (2001)

L3.12. B.Georgeot and D.L.Shepelyansky, *Quantum computer inverting time arrow for macroscopic systems*, Eur. Phys. J. D **19**, 263 (2002)

L3.13. G.Benenti, G.Casati, S.Montangero and D.L.Shepelyansky, *Efficient quantum computing of complex dynamics*, Phys. Rev. Lett. **87**, 227901 (2001)

L3.14. G.Benenti, G.Casati, S.Montangero and D.L.Shepelyansky, *Eigenstates of operating quantum computer: hypersensitivity to static imperfections*, Eur. Phys. J. D **20**, 293 (2002)

L3.15. A.D.Chepelianskii and D.L.Shepelyansky, *Simulation of chaos-assisted tunneling in a semiclassical regime on existing quantum computers*, Phys. Rev. A **66**, 054301 (2002)

L3.16. M.Terraneo and D.L.Shepelyansky, *Imperfection effects for multiple applications of the quantum wavelet transform*, Phys. Rev. Lett. **90** 257902 (2003)

L3.15. K.M.Frahm, R.Fleckinger and D.L.Shepelyansky, *Quantum chaos and random matrix theory for fidelity decay in quantum computations with static imperfections*, Eur. Phys. J. D **29**, 139 (2004)

References (continued):

L3.16. A.A.Pomeransky, O.V.Zhirov and D.L.Shepelyansky, *Phase diagram for the Grover algorithm with static imperfections*, Eur. Phys. J. D **31**, 131 (2004)

L3.17. J.W.Lee and D.L.Shepelyansky, *Quantum chaos algorithms and dissipative decoherence with quantum trajectories*, Phys. Rev. E, **71**, 056202 (2005)

L3.18. I.Garcia-Mata, K.Frahm and D.L.Shepelyansky, *Shor's factorization algorithm with a single qubit and imperfections*, Phys. Rev. A **78**, 062323 (2008)

L3.19. O.V.Zhirov and D.L.Shepelyansky, *Synchronization and bistability of qubit coupled to a driven dissipative oscillator*, Phys. Rev. Lett. **100**, 014101 (2008)

L3.20. O.V.Zhirov and D.L.Shepelyansky, *Quantum synchronization and entanglement of two qubits coupled to a driven dissipative resonator*, Phys. Rev. B **80**, 014519 (2009)

Books, reviews:

L3.B1. M.L.Mehta, *Random matrices*, Third edition. Pure and Applied Mathematics (Amsterdam), 142. Elsevier/Academic Press, Amsterdam, 2004

L3.B2. A.Bohr, B.R.Mottelson, Nuclear structure, Vol.1, Benjamin, N.Y. (1969).

L3.B3. V.Zelevinsky, B.A.Brown, N. Frazier, M.Horoi, *The nuclear shell model as a testing ground for many-body quantum chaos*, Phys. Rep. **276**, 85 (1996)

L3.B4. T.Guhr, A.Mueller-Groeling, H.A.Weidenmueller, *Random matrix theories in quantum physics: common concepts*, Phys.Rep. **299**, 189 (1998)

L3.B5. Y.Fyodorov, *Random matrix theory*, Scholarpedia **6(3)**, 9886 (2011)

References (continued):

L3.B6. A.Steane, *Quantum computing*, Rep. Prog. Phys. **61**, 117 (1998)
L3.B7. M.A.Nielson and I.L.Chuang, *Quantum computation and quantum information*, Cambridge Univ. Press (2000)
L3.B8. D.L.Shepelyansky, *Quantum chaos and quantum computers*, Nobel Symposium on Quantum Chaos Y2K (2000), Physica Scripta **T90**, 112 (2001)